HIGH PERFORMANCE POLYPROPYLENE NANOCOMPOSITES

by

Cüneyt Bağcıoğlu

B.S., in Chemistry, Boğaziçi University, 2005

Submitted to the Institute for Graduate Studies in
Science and Engineering in partial fulfillment of
the requirements for the degree of
Master of Science

Graduate Program in Chemistry
Boğaziçi University
2008

To my beloved family

ACKNOWLEDGEMENTS

I would like to express my sincere gratitude to my supervisor Prof. Nihan Nugay and also Prof. Turgut Nugay for their most valuable encouragement and guidance. I greatly appreciate their suggestions, continued support and enthusiasm that influence my personal development as a researcher. It was great pleasure for me to work with them.

I wish to thank to Assist. Prof. Nuri Ersoy for being one of the member of my examining committee, reviewing the manuscript and collaborating and making guiding comments through the project.

I sincerely thank to Dr. Osman G. Ersoy for his invaluable help and academic advice. I would also like to thank all the members of Material Research and Development Center in Arçelik/Tuzla and also M. Bora İşlier for his kind collaboration with this study.

I would like to express my special thanks to Dr. Sinan Şen for his valuable guidance and help in the laboratory and AFM measurements. I wish to thank my lab.-mates and then, Gökhan Çaylı, Dr. Bilge Gedik Uluocak and Aslı Çakır Saygılı for their help in obtaining TGA, ESEM, and XRD results, respectively. I would like to thank Hülya Metiner who is the heart of the department and all the members of the Chemistry Department for their encouragement and moral support during my research.

I'll always remember the support of all my friends. Even though there are many names I sincerely thank to Erhan Özkal, Sezgin Bayrak, Aydın Can, Kemal Kıraç, and Ahmet Recep Navruz for their both technical and moral support.

Finally, I would like to thank my beloved family, my parents and my pretty sister, for their unconditional support and encouragement during all my life.

This thesis has been supported by TÜBİTAK with the research project 106T073.

ABSTRACT

HIGH PERFORMANCE POLYPROPYLENE NANOCOMPOSITES

In recent years, polymeric nanocomposites received large attention due to their superior mechanical, thermal, and optical properties as compared to micro-composites and neat polymers. Therefore, the main objective of this study was to prepare and characterise high performance polypropylene nanocomposites (PPNCs) containing organophilic layered nanosilicate (Org-MMT) and compatibilizer (coupling agent) by means of melt extrusion in a twin-screw extruder in order to investigate the role of organoclay content and compatibilizer addition on nanocomposite structure, morphology, and mechanical properties.

Special attention was paid to design and synthesis of high performance polypropylene (PP) nanocomposites by choosing appropriate compatibilizers which are suitable for both stiffening/toughening and intercalation/exfoliation mechanisms. For this purpose, maleic anhydride grafted polypropylene (PP-g-MA) and maleic anhydride grafted ethylene-propylene-diene-monomer (EPDM-g-MA) were used as compatibilizers. Especially, the latter one is believed to serve as a special toughener coupling agent.

The resultant nanocomposites were characterized by using X-Ray Diffraction (XRD), Atomic Force Microscopy (AFM), Scanning Electron Microscopy (SEM), Thermogravimetric Analysis (TGA), Dynamic Mechanical Analysis (DMA) and Static Mechanical Analysis including Tensile and Flexural as well as Izod Impact Testing methods.

ÖZET

YÜKSEK PERFORMANSLI POLİPROPİLEN NANOKOMPOZİTLERİ

Polimerik nanokompozitler saf polimer ve mikro-kompozitlerle karşılaştırıldıklarında üstün mekanik, termal ve optik özelliklerinden dolayı son yıllarda büyük dikkat çekmektedir. Bu çalışmanın temel amacı, katmanlı organofilik nanosilika ve uyumlaştırıcı içeren yüksek performanslı polipropilen (PP) nanokompozitlerin, katılan organokil ve uyumlaştırıcının nanokompozit yapısı, morfolojisi ve mekanik özellikler üzerindeki rolünü incelemek amacıyla çift vidalı ekstrüderde eriyik ekstrüzyon yöntemiyle hazırlanması ve karakterizasyonudur.

Polipropilen (PP) nanokompozitlerinin hem mukavemet/darbe dayanımı hem de interkelasyon/eksfoliasyon için uygun uyumlaştırıcının seçimine dayalı dizaynı ve sentezine özel olarak dikkat edilmiştir. Bu yüzden, maleik anhidrit aşılı polipropilen (PP-g-MA) ve etilen-propilen-dien-monomer (EPDM-g-MA) uyumlaştırıcı olarak kullanılmıştır. Özellikle sonuncusunun özel darbe dayanımlılık uyumlaştırıcısı olarak görev yapabileceğine inanılmaktadır.

Elde edilen nanokompozitler X-ray kırınım (XRD), atomik kuvvet mikroskobu (AFM), taramalı elektron mikroskobu (SEM), termal Gravimetrik Analizi (TGA), dinamik mekanik analizi (DMA) ve çekme-germe, eğme ve Izod darbe test metodlarını içeren statik mekanik analizi ile karakterize edilmiştir.

TABLE OF CONTENTS

LIST OF FIGURES

LIST OF TABLES

LIST OF SYMBOLS / ABBREVIATIONS

A°	Angstrom
cm	Centimeter
D	Diameter
E’	Dynamic Storage Modulus
E”	Dynamic Loss Modulus
J	Joule
kg	Kilogram
kHz	Kilohertz
kN	Kilonewton
kV	Kilovolt
kW	Kilowatt
L	Length
min	Minute
μm	Micrometer
mm	Milimeter
MPa	Megapascal
Mwt	Molecular weight
Nm	Newtonmeter
nm	Nanometer
sec	Second
t	Thickness
Tan Delta (δ)	Loss Factor which is equal to E”/E’
T_g	Glass Transition Temperature
T_m	Melting Point
$T_{mix.}$	Mixing Temperature
w	Width
wt. %	Weight percent
χ_c	Crystallinity Degree

ΔH_f	Heat of Fusion
λ	Wavelength
θ	Incident Angle Theta

AFM	Atomic Force Microscopy
CEC	Cation Exchange Capacity
DMA	Dynamic Mechanical Analysis
DMF	N,N-Dimethyl Formamide
EPDM-g-MA	Maleic Anhydride grafted Ethylene-Propylene-Diene-Monomer
ESEM	Environmental Scanning Electron Microscope
HDPE	High density polyethylene
HDT	Heat distortion (deflection) temperature
LDPE	Low density polyethylene
MA	Maleic anhydride
MFI	Melt Flow Index
MMT	Montmorillonite
Org-MMT	Organo-modified Montmorillonite
PE	Polyethylene
PEO	Poly(ethylene) oxide
PET	Polyetylene terephthalate
PLSN	Polymer/Layered Silicate Nanocomposite
PMMA	Polymethylmetacrylate
PP	Polypropylene
PP-g-MA	Maleic Anhydride grafted Polypropylene
PPNC	Polypropylene Nanocomposite
PVA	Poly(vinyl alcohol)
rpm	Revolution per minute
SBS	Styrene-Butadiene-Styrene
SEBS-g-MA	Maleic Anhydride grafted Styrene-Ethylene-Butylene-Styrene

SEM	Scanning Electron Microscope
TEM	Transmission Electron Microscope
TGA	Thermogravimetric Analysis
THF	Tetrahydrofuran
WAXD	Wide-angle X-ray diffraction
XRD	X-Ray diffraction

1. INTRODUCTION

"Nanocomposite", as a term, is a description of two-phase material where one of the phases is dispersed in the second one on a nanometer (10^{-9} m) level. This term is frequently used in two distinct areas of material science: ceramics and polymers. However, only nanocomposites based on polymers will be considered in the scope of this research.

1.1. Polymer/Layered Silicate Nanocomposites (PLSN)

Polymers are incorporated with particles, as fillers, by manufacturers in order to improve the stiffness and toughness of the materials, to enhance their barrier properties and their resistance to fire and ignition or simply to reduce the cost. However, the addition of particulate fillers sometimes cause some drawbacks such as brittleness or opacity in the resulting composites [1].

Polymeric nanocomposites, being a new class of composites, are particle-filled polymers for which at least one dimension of the dispersed particles is in the nanometer range. Three types of nanocomposites can be distinguished depending on how many dimensions of the dispersed particles are in the nanometer range. When the three dimensions are in the order of nanometers, "isodimensional nanoparticles" such as spherical silica nanoparticles or semiconductor nanoclustors are considered. When two dimensions are in the nanometer scale and the third is larger, nanotubes; e.g, carbon nanotubes, or whiskers; e.g, cellulose whiskers, are dealt with. When only one dimension is in the nanometer range, the filler is present in the form of sheets of one to a few nanometer thick to hundreds to thousands nanometers long. This family of composites can simply be collected under the name of "polymer-layered crystal nanocomposites". These materials are particularly obtained by the intercalation of the polymer or a monomer subsequently polymerized inside the galleries of layered host crystals. A wide variety of

both synthetic and natural crystalline fillers are capable of intercalating a polymer under specific conditions [1]. Table 1.1 presents a list of some possible layered host crystals.

Table1.1. Example of layered host crystals susceptible to intercalation by a polymer [1]

Chemical nature	**Examples**
Element	Graphite
Metal chalcogenides	$(PbS)_{1.18}(TiS_2)_2$, MoS_2
Carbon oxides	Graphite oxide
Metal phosphates	$Zr(HPO_4)$
Clays and layered silicates	Montmorillonite, hectorite, saponite, fluromica,fluorohectorite, vermiculite, kaolinite, magadiite,…
Layered double hydroxides	$M_6Al_2(OH)_{16}CO_3.nH_2O$; M=Mg, Zn

Among all the potential nanocomposite filler precursors, the ones based on "clay and layered silicates" have been more widely investigated because of the ease of availability and their well-known intercalation chemistry [2-4] of the starting clay/layered silicate materials.

Although polymer/layered silicate nanocomposites were reported in the patent literature as early as 1950 [5] they have recently attracted great interest both in industry and in academia, since they often exhibit significant improvement in material properties as compared to neat polymer or conventional micro-and macro-composites [6] They have shown the dramatic enhancements in physical, thermal and mechanical properties even with a low loading of layered silicate [1, 7, 8]. The enhanced properties including tensile/flexural strength, heat deflection temperature (HDT), thermal stability, flame retardancy, barrier properties, and so on are reasonably increased due to the synergistic effects of the nano-scale structure and the maximized interaction between the fillers and polymer molecules.

Successful leading work on polymer/layered silicate nanocomposites was performed on the nylon-6/montmorillonite (MMT) clay system by Toyota research group [9-10]. They were successfully introduced an automotive timing-belt cover made from this nylon-6/MMT (layered silicate) nanocomposite as a commercial application.

Since then, in the light of this pioneering work, using the same concept other polymer/layered silicate nanocomposites systems, in which the polymer matrix includes polyolefins, epoxy resin, polyesters, polyamides, polyimide, styrenic polymers, polyurethanes, polycaprolactone, and acrylic polymer and so on were reported [6]. On the other hand, the formation of polymer/layered silicate nanocomposites was entirely reviewed by Lagaly [11], Akelah [12], Giannelis [13], Pinnavaia [14], and Mülhaupt [15].

Today polymer/layered silicate nanocomposites with their enhanced properties, weight reduction, and low cost benefits can find a particular place in some commercial applications. Besides being used in automotive parts, industries especially in Japan and USA are also developing nanocomposite barrier films for food packaging and other applications. Potential applications include airplane interiors, fuel tanks, and components in electrical or electronic parts, under-the-hood structural parts, breaks and tires.

1.1.1. Structure and Properties of Layered Silicates

The layered silicates most commonly used in preparation of polymer/layered silicate nanocomposites belong to the same structural family known as the 2:1 layered silicates (two tetrahedral sheets are present for one octahedral sheet) or phyllosilicates [16]. Their crystal structure consists of layers made up of two tetrahedrally coordinated silicon atoms fused to an edge-shared octahedral sheet of either aluminum or magnesium hydroxide. The layer thickness is around 1 nm and the lateral dimensions of these layers may vary from 30 nm to several microns or larger, depending on the particular layered silicate. These layers organize themselves to form stacks with a regular *Van der Waals gap* between them called the *interlayer* or *gallery*. Isomorphous substitution within the layers; as an example Al^{3+} replaced by Mg^{2+} or Mg^{2+} replaced by Li^{+}, generates negative charges

that are counterbalanced by alkali or alkaline earth cations situated inside the galleries [1, 2]. As the forces that hold the stacks together are relatively weak, the intercalation of small molecules between the layers is easy [2]. In order to make these phyllosilicates more organophilic, the hydrated cations present in the galleries can be exchanged with cationic surfactants such as alkylammonium or alkylphosphonium (onium). The modified clay, or "organoclay", being *organophilic,* its surface energy is lowered and is more compatible with organic polymers.

Montmorillonite (MMT), hectorite and saponite are the most commonly used layered silicates. Their structure and their chemical formula with characteristic parameters are given in Figure 1.1 and Table 1.2, respectively.

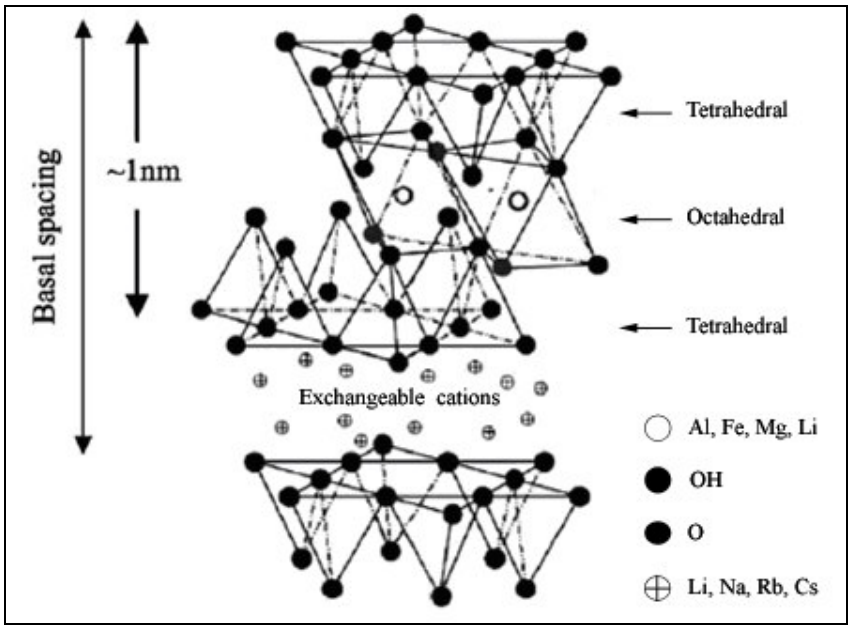

Figure 1.1. The structure of 2:1 phyllosilicates (e.g,. MMT) [6]

This type of layered silacate is characterized by a moderate negative surface charge kown as the "cation exchange capacity" (CEC), and generally expressed as meq/100g. This charge of the layer in not locally constant; that is to say, it varies from layer to layer and thus it must be considered as an average value over the whole crystal. Even if a small part of the charge balancing cations is located on the external crystallite surface, the majority of these exchangeable cations is located inside the galleries. When the hydrated

cations are ion-exchanged with organic cations such as bulkier alkylammonium ions, a larger interlayer spacing usually results in.

Table1.2. Chemical formula and characteristic parameter of commonly used 2:1 phyllosilicates. [6]

2:1 phyllosilicates	**Chemical formula**	**CEC (meq/100g)**	**Particle length (nm)**
Montmorillonite	$M_x(Al_{4-x}Mg_x)Si_8O_{20}(OH)_4$	110	100-150
Hectorite	$M_x(Al_{6-x}Mg_x)Si_8O_{20}(OH)_4$	120	200-300
Saponite	$M_xMg_6(Si_{8-x}Al_x)O20(OH)_4$	86.5	50-60

[a]M=monovalent cation; x=degree of isomorphous substitution (between 0.5 and 1.3)

Two particular characteristics of layered silicates that are generally considered for polymer/layered silicate nanocomposites. The first one is the ability of silicate particles to disperse into individual layers. The second feature is the ability to fine-tune their surface chemistry through ion-exchange reactions with organic cations. Since the degree of dispersion of layered silicate in a particular polymer matrix depends on the interlayer cation, these two characteristics are strongly related to each other.

1.1.2. Structure and Properties of Organically Modified Layered Silicates

The physical mixture of a polymer and layered silicate may not form a nanocomposite. This situation is the same as polymer blends and mostly separation into discrete phases takes place. In immiscible systems, which typically correspond to the conventionally filled polymers, the weak physical interaction between the organic and inorganic components leads to poor mechanical and thermal properties. Conversely, strong interactions between the polymer and the layered silicate in polymer layered silicate nanocomposites (PLSNs) result in the organic and inorganic phases being dispersed at the nanometer level. As a consequence, nanocomposites exhibit unique properties not shared by their micro- counterparts or conventionally filled polymers.

Pristine layered silicates usually contain hydrated Na^+ or K^+ ions. It is clear that, in this untreated state, layered silicates are only miscible with hydrophilic polymers such as poly(ethylene oxide) (PEO) or poly(vinyl alcohol) (PVA). To render layered silicates miscible with other polymer matrices, the normally hydrophilic silicate surface must be converted to an organophilic one, making the intercalation of many engineering polymers possible. This can generally be achieved by ion-exchange reactions with cationic surfactants including primary, secondary, tertiary, and quaternary alkylammonium or alkylphosphonium cations as shown in Figure 1.2. These cations in the organosilicates lower the surface energy of the inorganic host and improve the wetting characteristic of the polymer, and result in a larger interlayer spacing. In addition to these, the alkylammonium or alkylphosphonium cations can provide functional groups that can react with the polymer matrix, or in some cases initiate the polymerization of monomers to improve the strength of the interface between the inorganic host and the polymer matrix [17-22]

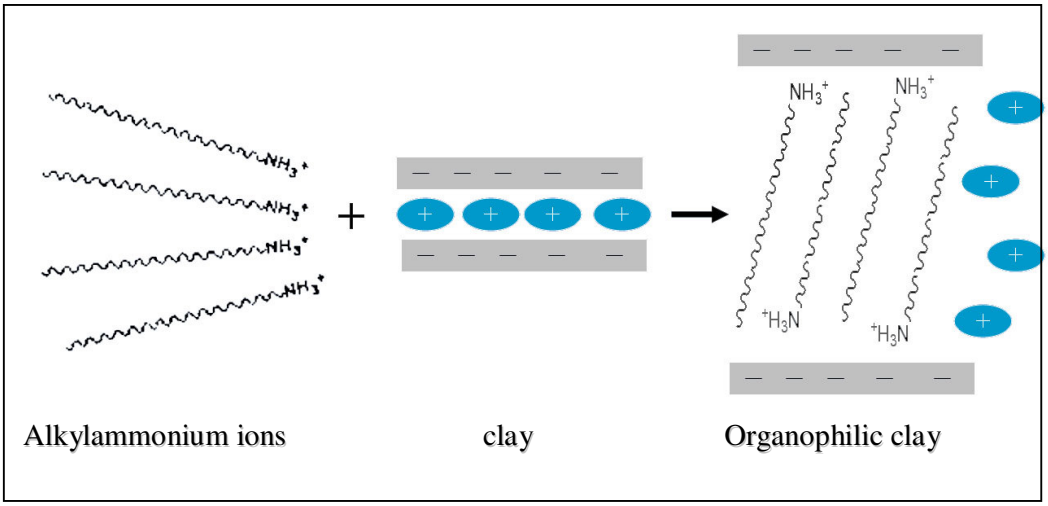

Figure 1.2. The cation-exchange process between alkylammonium/alkylphosphonium ions and cations initially intercalated between the clay layers. [23]

In order to describe the structure of the interlayer in organically modified layered silicates (simply, "*organoclays*") it has to be known that, as the negative charge originates in the silicate layer, the cationic head group of the alkylammonium molecule preferably resides at the layer surface, leaving the organic tail spreading away from the surface. In a

given temperature range, the cation exchange capacity of the layered silicate and the chain length of the organic tails define the equilibrium layer spacing. Depending on the X-ray diffraction (XRD) data, which is the traditional structural characterization technique used to determine the orientation and arrangement of the alkyl chain, the organic chains were thought to lie either parallel to the silicate layers forming mono or bilayers or spread away from the silicate layers forming mono or bimolecular "paraffinic" arrangements [24] as shown in Figure 1.3.

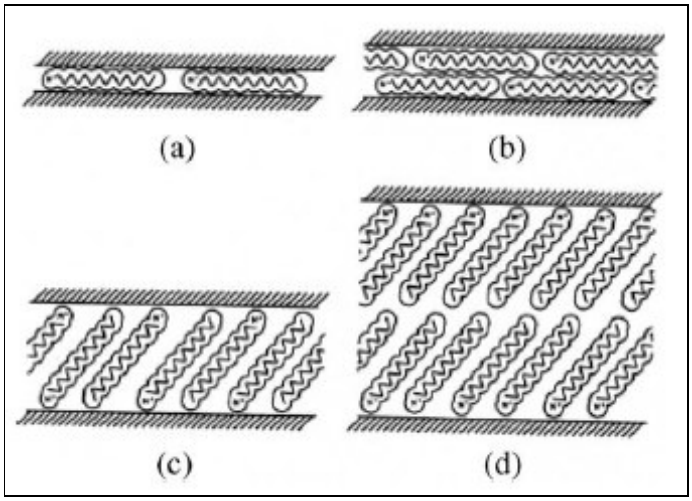

Figure 1.3. Alkyl chain aggregation (arrangement) in layered silicates: (a) lateral monolayer; (b) lateral bilayer; (c) paraffin-like monolayer; (d) paraffin-like bilayer. [1]

1.1.3. Types of Nanocomposites

Beyond the conventional approach, in which the polymer and layered silicate particles remain immiscible or phase separated; i.e., the polymer is unable to intercalate between the silicate layers, depending on the nature of the components used such as layered silicate, organic cation, and polymer matrix and the method of preparation, two types of nanocomposites are possible: *intercalated* nanocomposites and *exfoliated* or *delaminated* nanocomposites. "Intercalation" is a state in which the extended polymer chains are present between the clay layers, and this results in the well-ordered multi-layered structure with alternating polymer and inorganic layers and a repeated distance of a few nanometers. However, "exfoliation" is the state in which the silicate layers are

completely separated and uniformly dispersed in a continuous polymer matrix (see Figure 1.4).

The exfoliated or delaminated state is the most desirable because exfoliation creates individual clay platelets which are approximately 1 nm thick and have very high aspect ratio (large length/thickness ratio) of approximately 10-1000. Additionally, nanometric dispersion of layered silicate platelets provides a maximization of the interfacial region between the filler and the polymer matrix, and a consequent improvement in reinforcement effect.

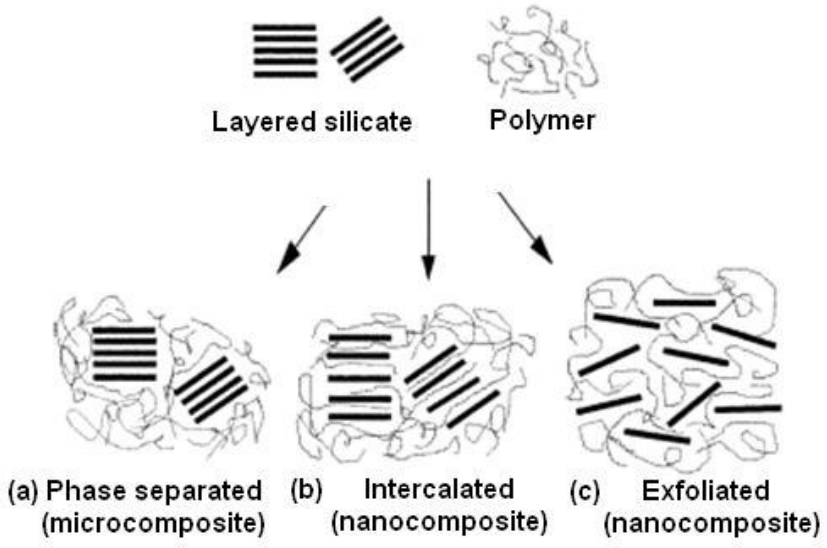

Figure 1.4. Scheme of different types of composites arising from the interaction of layered silicates and polymers. [1]

In general, two complementary techniques are used in order to characterize the abovementioned structure of nanocomposites. These are, typically, X-ray diffraction (XRD) analysis and transmission electron microscopy (TEM).

XRD is most commonly used to examine the nanocomposite structure due to its easiness and availability. By monitoring the position, shape, and intensity of the basal

reflections from the distributed silicate layers, the nanocomposite structure (namely, *intercalated* or *exfoliated*) may be identified. In *intercalated* nanocomposites, the repetitive multilayer structure is well-preserved, allowing the interlayer spacing to be determined. The intercalation of the polymer chains usually increases the interlayer spacing, in comparison with the spacing of the organically modified layered silicate used, leading to a shift of the diffraction peak towards lower angle (2θ) values (Figure 1.5) On the other hand, in *exfoliated* nanocomposites, no more diffraction peaks are observed in the XRD diffractogram This is because either too large spacing between the layers (i.e., exceeding 8 nm) or the nanocomposite does not present ordering anymore.

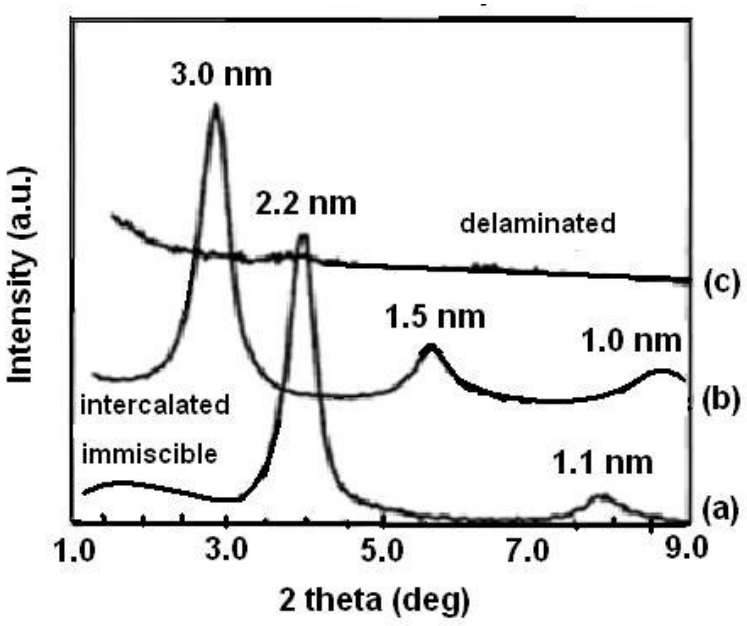

Figure 1.5. XRD patterns of (a) phase separated microcomposite; (b) intercalated nanocomposite and (c) exfoliated nanocomposite [1]

XRD offers a convenient method for determining the interlayer spacing of the silicate layers in the original layered silicates and in the intercalated nanocomposites within 1-4 nm. However, no more further information can be gathered about the spatial distribution of the silicate layers or any structural non-homogeneity in nanocomposites. In addition, some layered silicates initially do not exhibit well-defined basal reflections. Thus, peak broadening and intensity decreases are very difficult to study systematically.

Thus, conclusions related with the mechanism of nanocomposites formation and their structures based only on XRD patterns are not so definite.

TEM (Transmission Electron Microscopy) is complementarily used to characterize the nanocomposite morphology. It is a powerful technique to confirm the results obtained by XRD about the organization of nanostructures of the silicate layers in the nanocomposite. It allows a qualitative understanding of the internal structure, spatial distribution of the various phases, and views of the defect structure through direct visualization. Even though TEM gives a direct measure of the spatial distribution of the layers, it requires substantial skills in specimen preparation and analysis. Figure 1.6a and b show the TEM micrographs of intercalated and exfoliated nanocomposites, respectively.

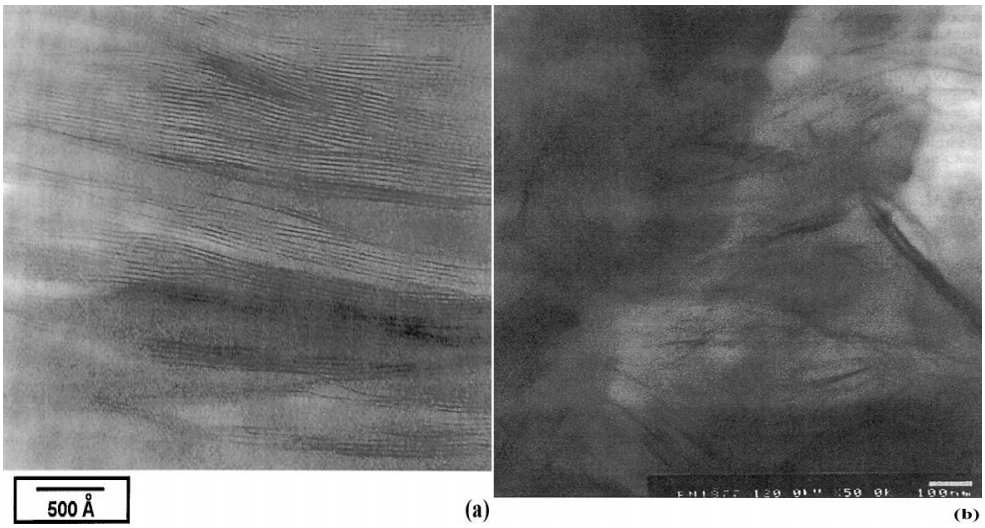

Figure 1.6. TEM micrographs of an (a) intercalated structure,(b) exfoliated structure [1]

1.1.4. Synthesis of Polymer-Layered Silicate Nanocomposites

Several methods have been used to prepare polymer-layered silicate nanocomposites. There are three main preparative methods that can be considered according to the starting materials and processing techniques.

1.1.4.1 In-Situ Polymerisation Method. In-situ polymerization was the first method used to synthesise polymer-layered silicate nanocomposites based on polyamide 6. In recent days, it is the conventional process used to synthesise thermoset polymer-clay nanocomposites. The strategy is described schematically in Figure 1.7.

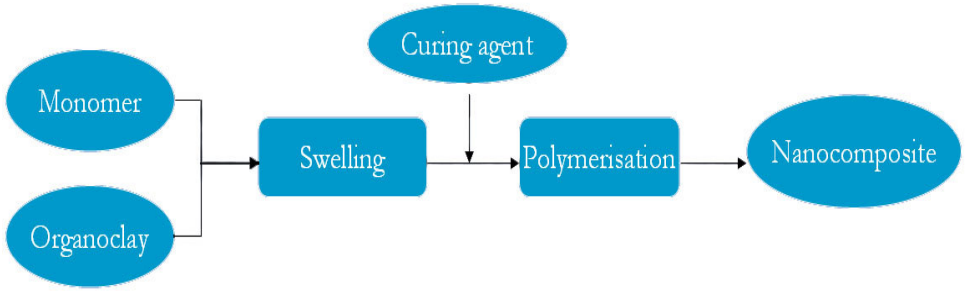

Figure 1.7. Flowchart presenting the different steps of the "in-situ polymerization" approach [23]

In this method, organically modified layered silicate (organoclay) is firstly swollen within the liquid monomer or a monomer solution. A certain amount of time is required for this step that depends on the polarity of the monomer molecules, the surface treatment of the organoclay, and the swelling temperature. Then, polymerization can be initiated either by heat or curing agent so, the polymerization can occur between the existing intercalated layers.

The key point of this method is to control the polymerization occurring between the layers. If the cure kinetics between the layers (intragallery polymerization) is lower than that of the outside layers (extragallery polymerization) the desired delamination of the layered silicate can not be achieved. That's why, the intragallery polymerization must be favoured as compared to the extragallery polymerization.

In addition, the driving force of the "in-situ polymerization" method is fairly associated with the polarity of the monomer molecules. That is to say, during the swelling step, the high surface energy of the layered silicate attracts the polar monomer molecules so that they diffuse between the clay layers. When equilibrium is reached, the diffusion

stops and the clay is swollen in the monomer to a certain extent corresponding to a perpendicular orientation of the alkylammonium ions as shown in Figure 1.8. When the polymerization is initiated, the monomer starts to react with the curing agent. This reaction lowers the overall polarity of the intercalated molecules and displaces the thermodynamic equilibrium so that more polar molecules are driven between the silicate layers leading to the delamination of the layered silicate.

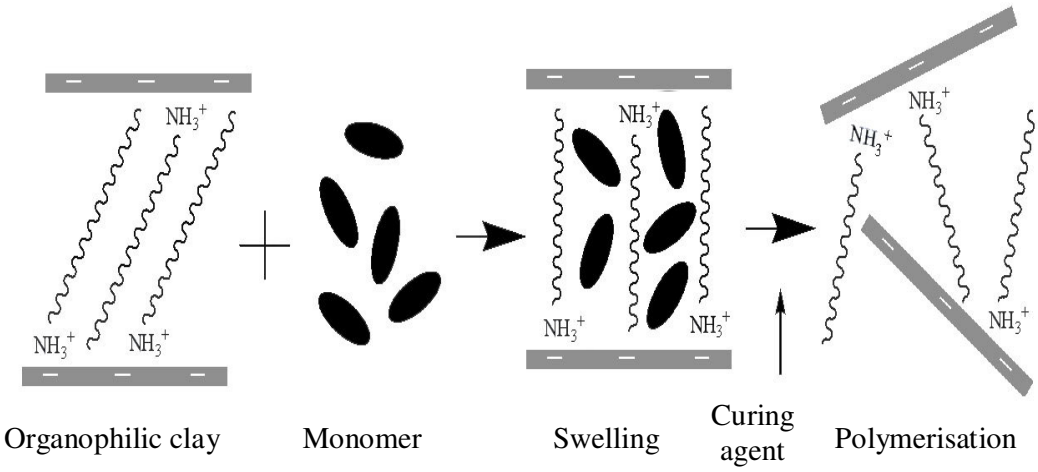

Figure 1.8. The "in-situ polymerization" method [23]

Polymer-layered silicate nanocomposites based on epoxy resin, unsaturated polyester, polyurethanes and polyethylene terephthalate (PET) have been synthesized by this method.

1.1.4.2 Solution Method. This method is based on a polar solvent system in which the polymer is soluble and the layered silicates are swellable. The strategy which is described in Figure 1.9 is the same as the previous preparative method

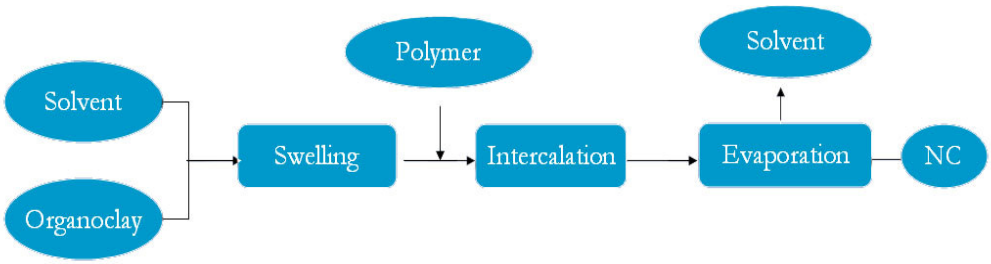

Figure 1.9. Flowchart presenting the different steps of the "solution" approach [23]

The organoclay is first swollen in a polar solvent, such as deionized water, chloroform, toluene, tetrahydrofuran (THF) or N,N-dimethylformamide (DMF). When the polymer and layered silicate solutions mixed, the polymer chains intercalate between the silicate layers displacing the solvent molecules. At the end, removing the solvent by evaporation usually under vacuum results in the intercalated polymer-layered silicate nanocomposite structure. Figure 1.10 simply shows how the polymer chains are intercalated between the silicate layers.

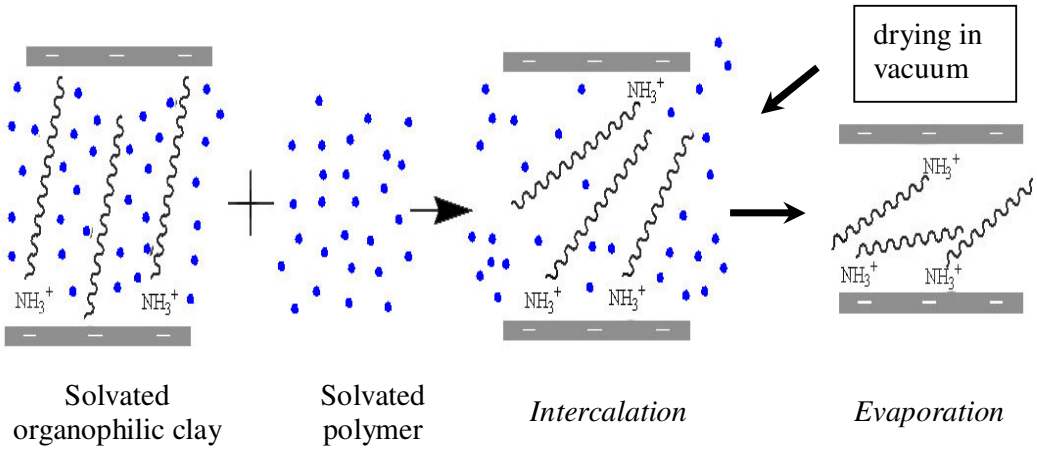

Figure 1.10. The intercalation of the polymer by the "solution" method [23]

Nanocomposites based on high-density polyethylene (HDPE), polimide, epoxy, poly(ethylene)oxide (PEO) or polymethylmethacrylate (PMMA) have been synthesized by this method.

The major advantage of this method is that it offers the possibilities to synthesise intercalated nanocomposites based on polyners with low or even no polarity. However, the "solution method" is difficult to apply in industry due to problems associated with the use of large quantities of solvent.

1.1.4.3 Melt Intercalation Method. This process which involves blending a molten thermoplastic with an organoclay and then, annealing, statically or under shear, at a temperature above the glass transition (softening) temperature of the polymer and finally

forming a nanocomposite was first reported by Vaia and Giannelis [18] in 1993. Figure 1.11 represents the melt intercalation strategy as a flowchart.

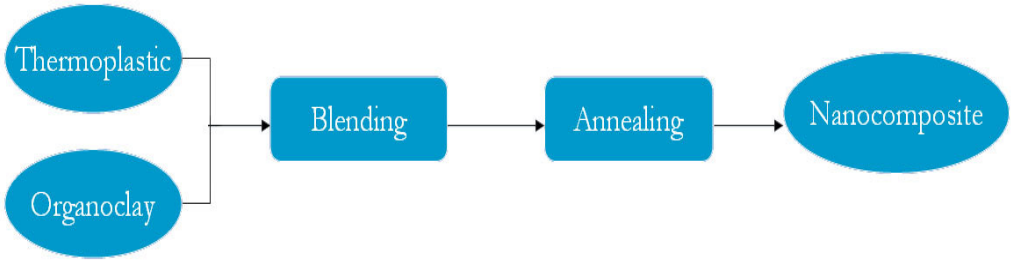

Figure 1.11. Flowchart presenting the different steps of the "melt intercalation" approach [23]

As shown in Figure 1.12, the polymer chains experience a dramatic loss of conformational entropy during the intercalation. The proposed driving force for this mechanism is the important enthalpic contribution of the polymer/organoclay interactions during the blending and the annealing steps.

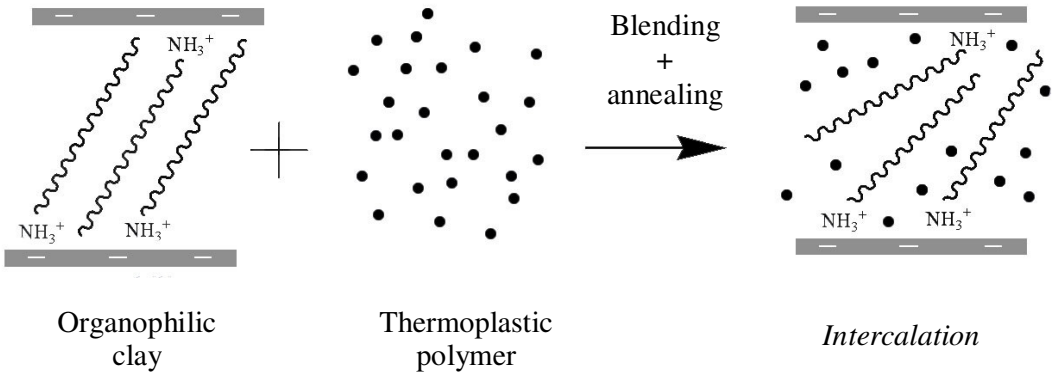

Figure 1.12. The "melt intercalation" process [23]

This method has great benefits over either in-situ polymerization or solution methods. First, this method is environmentally advantageous due to the absence of organic solvents. Second, it is compatible with current industrial processes, such as extrusion and injection molding. Finally, the melt intercalation method allows the use of wide range of polymers, from strongly polar polyamide 6 to polystyrene as well as polyolefins which

represent the biggest volume of polymers, which are not suitable for in situ polymerization or solution intercalation methods.

1.1.5. Properties of Polymer-Layered Silicate Nanocomposites

Nanocomposites consisting of a polymer matrix and a small amount of layered silicate (modified or not) (<10 wt%) frequently exhibit remarkably improved mechanical and material properties when compared to neat polymers. Improvements include a higher tensile/flexural modulus, increased strength and heat resistance (thermal stability), decreased gas permeability and flammability, and increased biodegradability of biodegradable polymers. The main reason for these improved properties in nanocomposites is the stronger interfacial interaction between the matrix and layered silicate, compared with conventional filler-reinforced systems.

Mechanical Properties : Presence of nanometer scale fillers in the polymer matrix significantly increases the mechanical properties of the nanocomposites compared to virgin polymer. For example, the tensile modulus of a polymeric material has been shown to be remarkably improved when nanocomposites are formed with layered silicates. In general, the main reason for this outstanding improvement in tensile modulus in nanocomposites is the strong interaction between the matrix and silicate layers via formation of hydrogen bonds. Although there are very few reports concerning the flexural properties, i.e., flexural modulus, flexural strength and etc…, it is observed that there was a significant increase in flexural modulus and flexural strength in synthesized nanocomposites compared to that of neat polymers. In addition, dynamic mechanical analysis measures the reponse of a given material to a cyclic deformation (usually tension or three point flexion type deformation) as a function of temperature. DMA results are composed of three main parameters: (a) the storage modulus (E'), corresponding to the elastic response to the deformation; (b) the loss modulus (E"), corresponding to the plastic response to the deformation, and (c) tan δ, that is the (E"/E') ratio, useful for determining the occurrence of molecular mobility transitions such as the glass transition temperature.

Thermal stability : The thermal stability of polymeric materials is usually studied by thermogravimetric analysis (TGA). The weight loss due to the formation of volatile products after degradation at high temperature is monitored as a function of temperature. When the heating is operated under an inert gas flow (nitrogen, helium etc…), a non-oxidative degradation occurs while the use of air or oxygen allows to follow the oxidative degradation of the sample. Generally, the incorporation of layered silicate into the polymer matrix was found to enhance thermal stability by acting as a superior insulator and mass transport barrier to the volatile products generated during decomposition.

Flammability and Fire Redardance : The cone calorimetry is one of the most effective method for studying the flammability and the fire retardant properties of polymeric materials. The flame retardant effect of nanocomposites mainly arises from the formation of char layers obtained through decomposition. This multi-layered silicate structure may act as an excellent insulator by slowing down the escape of the volatile decomposition products. Whatever the nature of the matrix (thermoplastics and thermosets) and whatever the structure of the nanocomposite (exfoliated or intercalated), always the same interlayer spacing was found for the recovered chars as analysed by XRD. This means that nanocomposite parts conserve their shape during combustion as well. As a consequence, showing the highest char yield and a self-extinguishing behavior polymer-layered silicate nanocomposites propose a new environmentally favourable approach to improve fire resistance of polymers.

Gas Barrier Properties : Layered silicates are believed to increase the barrier properties by creating a labyrinth or 'tortous path' that retards the passage of the gas molecules through the matrix. Figure 1.13 shows the formation of this tortuous path. The direct benefit of the formation of such a path is clearly observed in polyimide/clay nanocomposites by dramatically improved barrier properties, with simultaneous decrease in the thermal expansion coefficient [25]. Moreover, the high aspect ratio characteristic of nanolayers especially in exfoliated nanocomposites has been found to highly reduce the gas permeability (small gas molecules such as O_2, H_2O, He, CO_2 etc..) in films prepared from such nanomaterials.

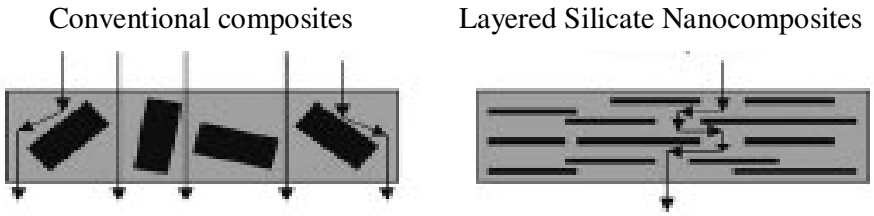

Figure 1.13. Formation of tortuous path in PLSNs. [6]

Although layered silicates are microns in length, they are just 1 nm thick. Thus, when single layers are dispersed in a polymer matrix, the resulting nanocomposite is optically clear in visible light. That is, the visible region is not affected by the presence of the silicate layers and retains the high transparency of correspondimg polymer matrix.

1.1.6. Applications of Polymer-Layered Silicate Nanocomposites

The nanocomposites have already been used widely in the various fields of injection molding, e.g., engine cover, timing belt cover, oil reservoir tank; and fuel hose in automobile industry, floor adjuster and handrail in the construction fields and various connectors in the electrical fields. Since nylon 6/layered silicate nanocomposites show a high modulus and heat distortion temperature (an index of heat resistance towards applied load) [26], the automotive timing belt covers made from these nanocomposites by injection molding was the first example of industrialized use of polymer-layered silicate nanocomposites. Nylon 6/layered silicate nanocomposites also have high gas barrier property due to the the nanometer level dispersion of silicate layers. This property enables them being also used in food packaging films in a wide range of applications.

As mentioned above, the increased mechanical properties and dimensional stability make the nanocomposites more convenient to be used as high value construction materials. They are highly stable against aggressive chemicals. Thus, they can also be used in corrosive protective coatings.

Another reason why polymeric nanocomposites are widely used in packaging and automotive industries is the decreased permeability for gases and water, as well as for hydrocarbons. In high temperature areas such as internal combustion engines, nanocomposites are more attractive and promising than other conventional materials because of their enhanced thermal stability, flame retardancy, and heat distortion temperature. These materials have a good prospect of application for the near future in daily life. Therefore, the art of nanocomposites may be considered as another alternative to the production of the high-tech composites which are both expensive and labor-intensive. By extrusion technology, lower labor-intensive mass production lines are expected in future.

1.2. Polypropylene-Layered Silicate Nanocomposites

In the past decade, especially with the development of nylon 6/clay nanocomposites achieved by Toyota group [27, 28], research on the preparation and characterization of polymer nanocomposites has attracted much academic and industrial attention . Among the nanocomposites investigated, polymer/layered silicate systems have exhibited great promise for industrial applications because of their potential to display synergistically advanced properties with only minor amounts (e.g., 3 ~ 5 wt %) of layered silicate loading.

Currently, study of PP nanocomposites (PPNC) has attracted the interest of many researchers because of huge commercial opportunities in both automotive and packaging industries. Polypropylene exhibits an attractive combination of low cost, low weight, and extraordinary versatility in terms of properties, applications, and recycling [29] To improve the competitiveness of PP in engineering resin applications, it is important to increase the dimensional stability, stiffness, strength, and impact resistance. Therefore, special attention is being placed on the development of nanofilled PP nanocomposites.

1.2.1. Polypropylene (PP)

Polypropylene, with the chemical formula $(C_3H_6)_x$ (see Figure 1.14), is a thermoplastic polymer used in a wide variety of applications including packaging, plastic parts, laboratory equipment, automotive components etc. Crystallinity property and Young's Modulus of polypropylene is between that of low density polyethylene (LDPE) and high density polyethylene (HDPE). It is less tough but also less brittle than HDPE, this allows polypropylene to be used as an engineering plastic. Resistance to fatigue, high melting point (130-168 ˚C) and relatively low cost are the other superior properties of PP.

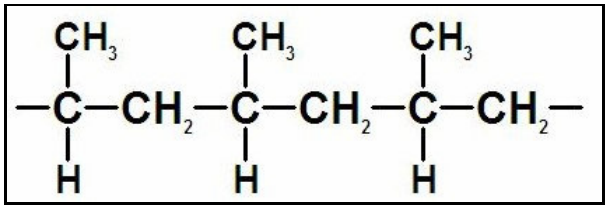

Figure 1.14. Molecular structure of polypropylene chain.

Due to its non-polar nature, PP has high resistance to most solvents and chemicals and also good resistance to moisture. Non-polar structure also makes PP hydrophobic and makes polar clay minerals and layers difficult to disperse in it. Its highly crystalline nature provides high tensile strength, stiffness and surface hardness to PP.

1.2.2. Organo-Modified Montmorillonite (Org-MMT)

One of the most commonly used organically modified layered silicates is derived from "montmorillonite" (MMT). Its structure is made of several stacked layers, with an individual layer thickness around 1 nm and a lateral dimension of 100-200 nm. These layers organize themselves to form the stacks with a regular gap between them.

Even though MMT is recognized as an appropriate choice for preparing high performance PP nanocomposites, since it is hydrophilic in nature, it is difficult to exfoliate in PP matrix. That is, to form/synthesise a PP nanocomposite, the layered silicates must be dispersed finely and uniformly in PP matrix. Therefore, the surface treatment of silicate

layers (organomodification) is necessary to render its surface more hydrophobic, which facilitates exfoliation. In general, this can be achieved by ion-exchange reactions with cationic surfactants including mostly quaternary alkylammonium cations [1, 6, 23]. This organomodification both leads to an expansion of the basal spacing between the silicate layers due to the presence of alkyl chain intercalated in the interlayer and increases the compatibility between the hydrophobic PP matrix and the hydrophilic MMT silicates.

1.2.3. Compatibilizers

Polypropylene is one of the most widely used plastics in large volume. To overcome the disadvantages of PP, such as low toughness and low service temperature, and to enhance the thermal stability, scientists have tried to improve its properties with nanotechnologies. Using melt intercalation, a suitable layered silicate can be compounded with PP to obtain a nanocomposite [1]. In order to improve the compatibility between the non-polar PP and the polar layered silicate, the latter is generally modified with long organic alkyl chains; this is called organo-modified layered silicate (organoclay). However, because of the difference in polarity of PP and organoclay, it is difficult to obtain an exfoliated structure of the filler in the polymer matrix during extrusion process. Efforts were made to improve the mixing of clay in PP by using functional oligomers as compatibilizers. Usuki et al. [48] first reported a novel approach to prepare PP nanocomposites using a functional oligomer (PP-OH) with polar telechelic OH groups as compatibilizer. Several studies [31-35] also reported the use of maleic anhydride grafted polypropylene (PP-g-MA) as compatibilizer via melt process. In both cases the interaction between filler and polymer is enhanced by a strong hydrogen bonding between OH or COOH groups and the oxygen groups of silicate.

As a result of these reports there are two important factors to achieve the exfoliation of the clay layer silicates: (1) the compatibilizer should be *miscible* with the polypropylene matrix, and (2) it should include a certain amount of *polar functional groups* in a molecule. Generally, the polypropylenes modified with maleic anhydride (MA) fulfill the two requirements and are frequently used as compatibilizer for polypropylene

nanocomposites. However, they have mechanical properties lower than the native polypropylene, due to chain scission during grafting which in turn resulting in lower mechanical properties of the final composite. Hence, it is important to investigate the effect of PP-g-MA on the degree of dispersion, to optimize its concentration. Moreover, the chemical properties of maleated PP (PP-g-MA) that influence its effectiveness as a compatibilizer for PP/organoclay nanocomposites are (1) *the molecular weight*, which determines the magnitude of the shear viscosity and melt flow index (MFI), and (2) *the MA content*, which is related to the amount of functionality present in the compatibilizer. The effect of the MA content on the clay dispersion has been studied extensively, but the results are somewhat inconsistent. A high MA concentration generally enhances the melt intercalation of PP oligomers into clay layers; however, it may lead to immiscibility with the PP matrix [31] and decrease in the mechanical properties of the composites. However, some authors have found that a high MA concentration (4.2%) improves the mechanical strength better than a low MA concentration (2.9%) with the same composition. [34] Because the mechanical properties are also affected by the compatibilizer loading, it is needed to be careful when assessing the results from different sources. Therefore, regardless of the type of maleic anhydride grafted polypropylene (PP-*g*-MA), the weight ratio of PP-*g*-MA to organoclay was roughly 3:1 so that the maximum improvement in the mechanical properties could be achieved [30]. As expected, too high a fraction of PP-*g*-MA is damaging to mechanical properties because the physical properties of compatibilizers are usually inferior to those of the polymer matrix, and too low a fraction of PP-*g*-MA makes it impossible to reach a desirable degree of clay dispersion. There is an optimum composition (up to 22% by weight) for individual maleated PP to be incorporated into PP/organoclay nanocomposites.

In addition to PP-g-MA, impact toughening compatibilisers are also used in melt processing of PP nanocomposites. One of the major deficiencies of PP and PPNC is low impact resistance, particularly at low temperatures. Blending PP with an elastomeric modifier may provide the way to improve the impact resistance of the base matrix. Lots of articles reviewing the advances in toughening mechanisms of PP/elastomer blends for the last 20 years were published [36]. Recently, in the PP nanocomposite area, ethylene propylene rubber (EPR), ethylene–propylene–diene monomer rubber (EPDM) and

ethylene-1-octylene copolymer (POE) are the most frequently used PP impact modifiers [37].

Moreover, the addition of layered silicates as fillers leads to a drastic decrease in the tensile ductility of the PP/Layered silicate nanocomposites. To improve the structural strength and prepare tougher materials, elastomer particle addition is essentially required. Hence, it is, alternatively, thought that the incorporation of a styrene-ethylene-butylene-styrene (SEBS) into the PP matrix can improve the tensile ductility and impact strength of the PP nanocomposites. SEBS elastomer particles have been extensively used to enhance the tensile ductility and toughness of conventional PP microcomposites [38]. The elastomer phase containing reactive groups and block copolymers that are compatible with the matrix can lead to finer dispersion of rubber particles in the polymer matrix. In this regard, Tjong and coworkers employed maleated styrene-ethylene-butylene-styrene (SEBS-g-MA) to toughen the PP and HDPE nanocomposites [39, 40] and it is reported that SEBS-g-MA addition improves the tensile ductility, hence impact strength of the resulting nanocomposites. However, intercalated or partially delaminated structures can only be obtained. Sue and coworkers used styrene-butadiene-styrene (SBS) rubber to toughen PP-clay system. The SBS is found to have good compatibility with clay particles, thereby promoting dispersion of clay particles in PP matrix [41].

1.3. Compounding Process: Extrusion and Twin-Screw Extruders

1.3.1. Extrusion and Twin Screw Extruders

Polymer melt intercalation is a promising method due to its high productivity, relatively lower cost and compatibility with current polymer processing techniques such as extrusion and injection molding. During extrusion process, the clay agglomerates are broken up by the external shear forces and the diffusion of polymer macromolecules into the clay galleries takes place [42].

A typical extrusion line consists of the material feed hopper, the extruder (drive, gearbox and screws), the extrusion die, the haul-off and a pelletizer.

The components of the extrusion line are regardless of the extruder type and a typical layout is shown in Figure 1. 15.

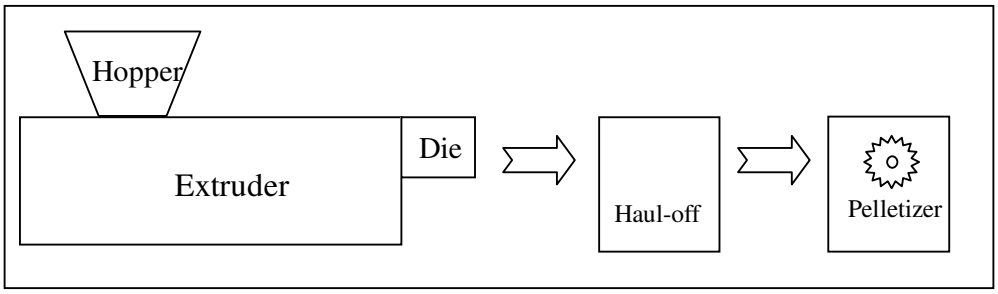

Figure 1.15. The basic components of an extrusion line.

The hopper stores the raw polymer (in either powder or granule form) and feeds it into the extruder. The extruder has preheated barrels and rotating screw(s) that transports the polymer from feeder to the die exit. Inside the extruder, the molten material is heated, mixed, pressurized and metered simultaneously. At the die the composite takes its final shape and is then cooled while being drawn along by the haul-off device. After cooling (either by water or air), the material is cut by a pelletizer.

Commonly used continuous screw extruders can be classified in two groups: Single screw and twin screw extruders. The former is the most basic form of extruder that simply melts and forms the material. In contrast, twin screw extruders provide excellent melt mixing and are widely used for polymer nanocomposite manufacturing with different types [43, 44] shown in Figure 1.16.

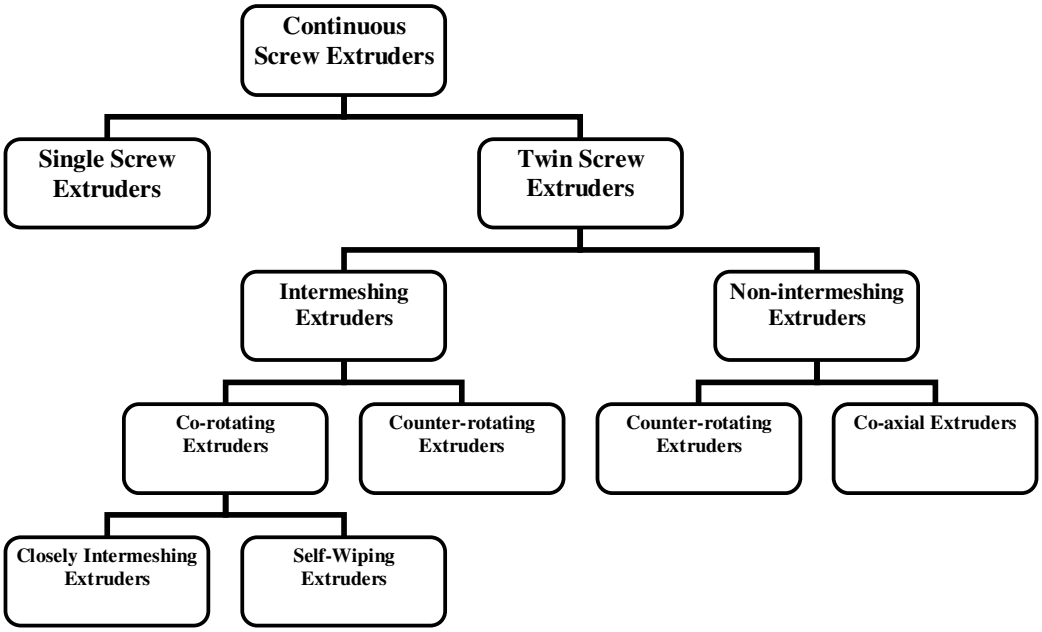

Figure 1.16. The main types of extruders.

In addition to this, twin screw extruders are more flexible due to their modular design of screw and barrel and they have better feeding, melting, mixing and degassing properties compared to single screw extruders [44].

Twin-screw extruders are used extensively in polymer blending and also in many applications such as processing of food, essential oils, paints, and many other highly viscous materials [45, 46]. They provide high shear rate and good mixing of compounding materials at a relatively short residence time. In twin-screw extruders, two screws lie adjacent to each other in a barrel casing a "figure-8-pattern" cross section (see Figure 1.17). As illustrated in the diagram above, twin-screw extruders are of many types, such as intermeshing, non-intermeshing, co-rotating, counter-rotating etc. When the screws rotate in the same direction they are called co-rotating but in the opposite direction, then they are known as counter-rotating twin-screw extruders. Twin-screw extruders are named as intermeshing or non-intermeshing depending upon the separation between the axes of their screws. If the distance between the axes is less than the diameter at the tip of the screw flight, then one screw intermeshes with the other and it is called intermeshing twin-screw extruder. If not it is a non-intermeshing twin-screw extruder. When the flights of one screw wipe the root of the other screw it is a self wiping twin-screw extruder [45]. A

drawing of a self-wiping co-rotating intermeshing extruder screws in Figure 1.17 will be explanatory about the screw geometry.

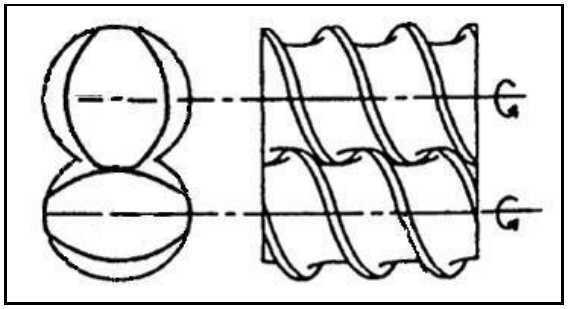

Figure 1.17. Screw geometry of a self-wiping co-rotating intermeshing extruder

2. AIM OF THE STUDY

The main objective of this study is to prepare and characterise high performance polypropylene nanocomposites (PPNCs) containing organophilic layered nanosilicate (Org-MMT) and compatibilizer by means of melt extrusion in a twin-screw extruder at 190 oC in order to investigate the role of organoclay content and compatibilizer addition on nanocomposite structure, morphology, and mechanical properties.

For this purpose, it is aimed to determine the proper compositions of control PPNCs including all three components, namely; PP, organoclay, and maleic anhydride grafted oligomer (PP-g-MA) and processing conditions in lab-scale internal mixer before scaling up to extruder conditions. Since the process depends critically on the characteristics of the ingredients, special attention is paid to formulation of PPNCs which greatly affect the structure, morphology and performance.

It was also targeted to prepare high impact and the most desired exfoliated polypropylene nanocomposites with enhanced properties including stiffness and toughness. The effects of adding varying amounts of special toughener compatibilizer such as EPDM-g-MA as well as organoclay loading on final performances of PPNCs were examined.

3. EXPERIMENTAL WORK

3.1. Materials

The polypropylene (PP) used for this study as a main polymer matrix was obtained from Borealis, the trade name of PP is "PP-Moplen HE125 MO", its melt flow (MFI) at 230 ^{o}C is 12,18 g/10 min, its melting point (T_m) is 168,13 ^{o}C, and its crystallinity degree (χ_c) is around 27,5%. Two different types of maleic anhydride grafted polypropylene (PP-g-MA) were used as compatibilizers. One of them purchased from DuPont de Nemours Int. with trade name Fusabond-M 613-05 and the other one was supplied from Mitsui Chemicals with trade name Admer-QF-300 E. Also, maleic anhydride grafted thermoplastic elastomer, namely, maleic anhydride grafted ethylene-propylene-diene-monomer (EPDM-g-MA), was used as toughener-compatibilizer. EPDM-g-MA (Trade name: Fusabond- MF-416 D), was purchased from commercial source. Table 3.1 shows the trade names and suppliers of all polymer materials used in this study.

Table 3.1. Polymer materials used in this study

Name	**Commercial name**	**Source**
Polypropylene (PP)	Moplen-HE 125 MO	Borealis
Maleic anhydride grafted polypropylene (PP-g-MA)	QF-300 E (ADMER)	Mitsui Chemicals
Maleic anhydride grafted polypropylene (PP-g-MA)	M 613-05 (FUSABOND)	DuPont de Nemours
Maleic anhydride grafted ethylene-propylene-diene-monomer (EPDM-g-MA)	FUSABOND- MF-416 D	DuPont de Nemours

To obtain more information on the compatibilizers, samples were characterized by dissolution in hot toluene and standard titration was performed to obtain some qualitative information which are given in Table 3.2.

Table 3.2. Analytical characterization results of grafted polymers

MA grafted polymers	V (ml KOH)	wt % MA content	[a]Acid number (mg of KOH/g of grafted polymer)
QF-300 E (PP-g-MA)	0,2	0,123	1,4
M 613-05 (PP-g-MA)	0,8	0,495	5,6
EPDM-g-MA	1,6	0,99	12,6

[a] The acid number (AN) of PP-g-MA is defined as the amount of potassium hydroxide that will react with the anhydride groups in PP-g-MA (mg of KOH/g of PP-g-MA).

Table 3.3 summarizes some basic determined properties of homopolymer PP and MA grafted polymers; namely, QF-300 E (PP-g-MA), M 613-05 (PP-g-MA) and EPDM-g-MA.

Table 3.3. Some properties of the PP matrix and compatibilizers used in the study

Polymer name	ΔHf (J/g)	* T_m (^{0}C)	% crystallinity	** MFI (g/10min)
Polypropylene (PP)	57,48	168,13	27,50	12,18
QF-300 E (Admer)	46,10	167,91	26,84	7,27
M 613–05 (Fusabond)	54,09	163,73	22,06	250
EPDM-g-MA	2,67	158,80	-	6,27

* Tm = melting point determined from the peak value of the DSC scan
** MFI = determined at 2,16 kg and 230^{o}C

NOTE: MFI (melt flow index) values of QF-300E & M-613 05 at 2,16 kg and 190 ^{o}C are 3,1 and 47,0 g/10 min, respectively.

The organically modified montmorillonite (Trade name: Nanofil-15) containing dimethyl dihydrogenated tallow quaternary ammonium (2M2HT) modifier with cation exchange capacity (CEC) of 100 meq/100 g was kindly provided by Süd-Chemie AG, Germany. The chemical structure of the dimethyl dihydrogenated tallow quaternary

ammonium modifier in which HT is made of approximately 65% $C_{18}H_{37}$, 30% $C_{16}H_{33}$, and 5% $C_{14}H_{29}$ is given in Figure 3.1.

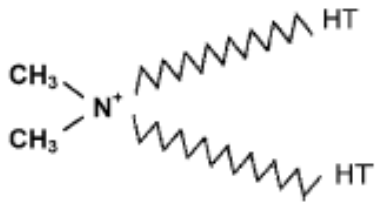

Figure 3.1. Chemical structure of the dimethyl dihydrogenated tallow quaternary ammonium chloride.

Montmorillonite layered silicate particles (pristine clay: 1080-Na^+MMT) and as received organically modified layered silicate particles (organoclay: Nanofil-15) were characterized with XRD to determine the basal spacing. The diffraction peaks and *d*-spacing of pristine clay and organoclay were tabulated in Table 3.4.

Table 3.4. XRD results of pristine clay and organoclay

Name	**Type of clay**	**d_{001} (nm)**	**2 θ (^{o})**
1080-Na^+MMT	Pristine clay	1,22 nm	7,250
Nanofil-15	Organoclay	2,93 nm	3,010

As can be seen in Figure 3.2, the peak of the pristine clay particles of 1080-Na^+MMT occurred at 2θ value of 7,250 with *d*-spacings of 1.22 nm. This peak was shifted to lower angles in organoclay, i.e., Nanofil-15, at about 2θ = 3,010 with a corresponding increase in the *d*-spacing as 2,93 nm. This result proves the effective existence of intercalant in MMT galleries. That is, the increase in the interlayer spacing of Nanofil-15 was attributed to the surfactant used. Onium ion modification is essential for making the clay particles organophilic and also for increasing their *d*-spacing. Specifically, Nanofil-15 is dimethyl dihydrogenated tallow quaternary ammonium ion (cationic surfactant) modified montmorillonite (MMT).

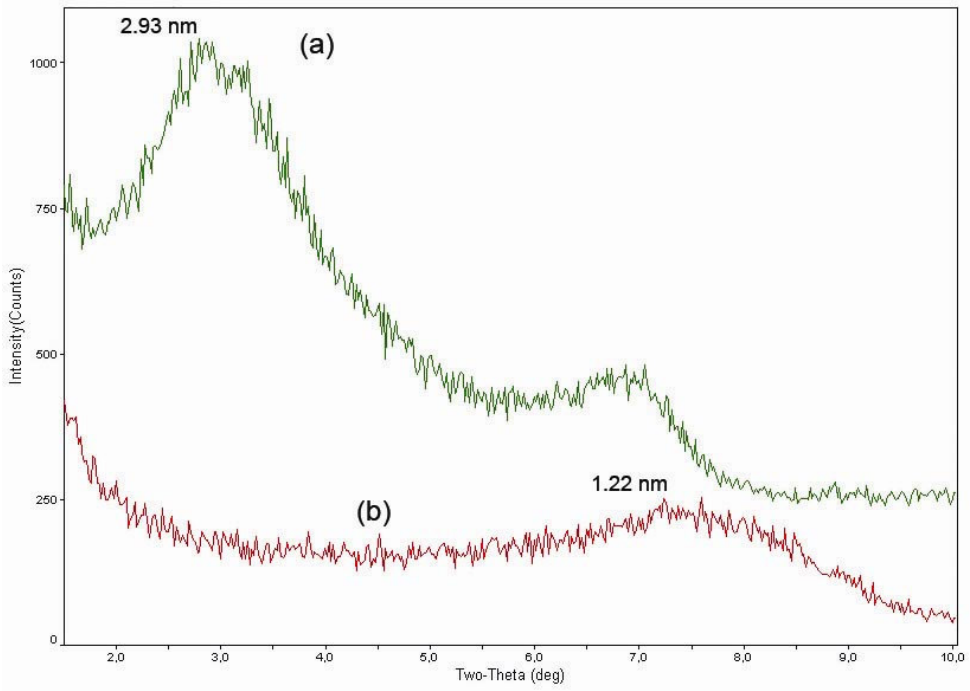

Figure 3.2. XRD patterns of organoclay (a) and pristine clay (b)

In order to examine the thermal degradation of the organic components of organically modified layered silicate "Nanofil-15" thermogravimetric analysis (TGA) was performed. Thermogravimetric analysis of organoclay, carried out in inert atmosphere (from room temperature to 600 ^{o}C, 10^{o}C/min), showed weight loss of about 38,5 % between 200 and 450 ^{o}C (Figure 3.3). This loss is due to the degradation of the organic fraction introduced as modifier in the clay as well as to the loss of hydration water.

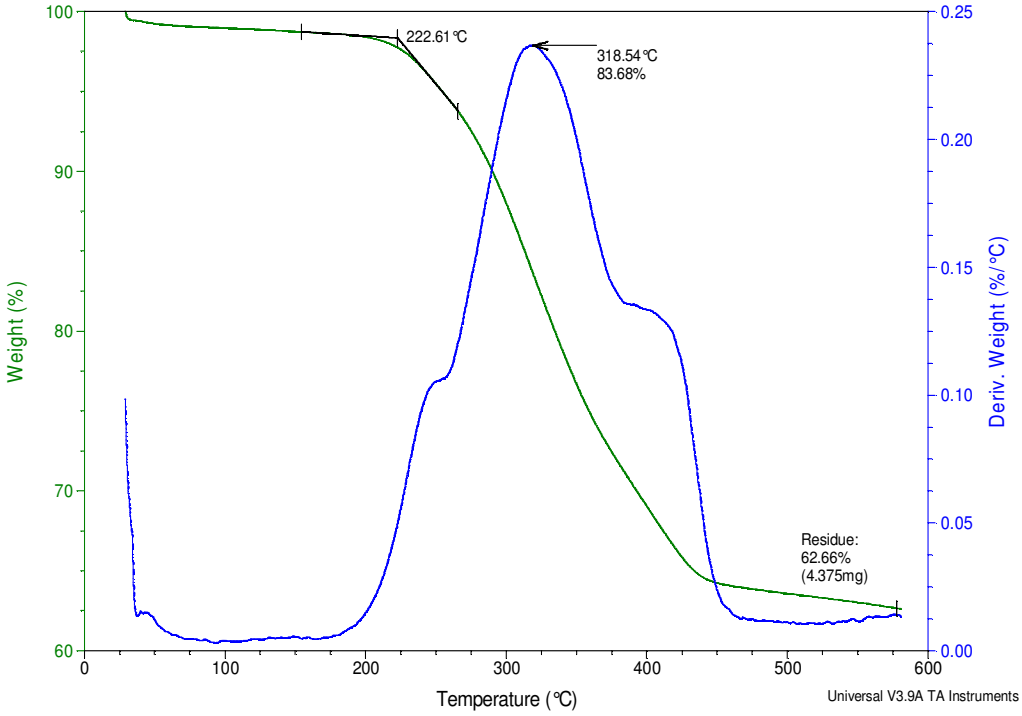

Figure 3.3. TGA curve of organoclay

3.2. Determination of Compounding Recipes in Internal Mixer

To determine the proper composition of the compatibilizers for the nanocomposites and critically compare the performances of the various compatibilizers such as PP-g-MA and EPDM-g-MA, we first employed an internal mixer (produced by METGÜR MAKİNA , Bursa-TÜRKİYE) for the melt compounding of organoclay, compatibilizers and PP matrix. Melt mixing of the samples was performed in this internal mixer (mixing volume: 50 cm^3) equipped with roller rotors (Figure 3.4). A dry batch of 40 g containing all three components (PP and Compatibilizer [PP-g-MA or EPDM-g-MA] and Organoclay) in powder or pellet form was pre-mixed before introduction into the internal mixer. The mixture was then added to this laboratory-scale internal mixer. It was compounded with following conditions: rotor speed N=60 rpm, mixing time t=15 min (during which the imposed torque and temperature reached an equilibrium value) and mixer temperature T_{mix}=190 ^oC (measured by an internal thermocouple). The mixing temperature was set at about the melting point of the base PP polymer matrix and/or

compatibilizers. For comparison, all nanocomposites were prepared by melt mixing under the same conditions (N=60 rpm, t=15 min, T_{mix}= 190 ^{o}C).

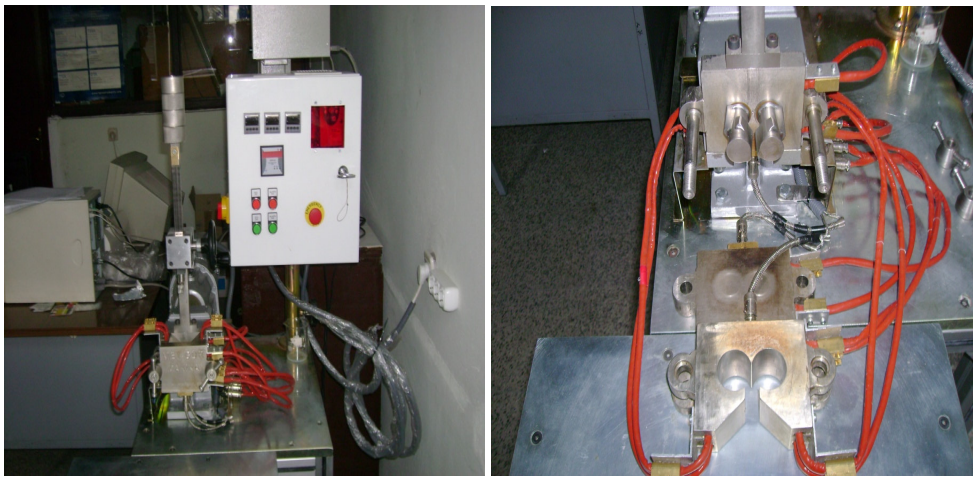

Figure 3.4. photograph of lab-scale internal mixer.

Several formulations were tried with varying organoclay loading such as 1, 3, 5, 7 %. Some of them were control blends that composed of just PP and organoclay or PP and corresponding compatibilizer. The nanocomposites with varying compatibilizer to organoclay ratio such as 1:1, 2:1, 3:1 were also prepared.

The dispersibility of the silicate layers in prepared PP nanocomposites in lab-scale internal mixer was evaluated by using the X-ray diffractometer. Thermogravimetric analysis of each prepared blends/nanocomposites were also performed simultaneously. As a result, in the light of gathered XRD and TGA data, in order to scale up the production, some of the selected formulations were carried out to twin-screw extruder in Arçelik (Çayırova/Tuzla).

3.3. Compounding in Twin-Screw Extruder and Specimen Preparation with Injection Molding Machine

After determining and selecting the proper compositions prepared in internal mixer, melt mixing of PP/Compatibilizer (PP-g-MA or EPDM-g-MA) /Nanofil-15 composites were also studied using a twin screw extruder. The machine used was an industrial self-wiping, co-rotating twin screw extruder, PRISM TSE 24 HC (The Netherlands) with following characteristics: with high shear screw configuration, screw diameter = 24 mm, L/D=28 (length/diameter ratio). In addition to the screw configuration, the principal processing variables were the throughput rate, screw speed, and barrel-temperature profiles. After a few trials, the screw speed was set at 500 rpm, and the barrel temperatures were set from 70°C at the first barrel to 190°C at the last barrel. The barrel-temperature profiles are also shown in Figure 3.5. The screw speed and the barrel temperatures were fixed for all the experimental runs. Moreover, the throughput rate was fixed at about 6 kg/h.

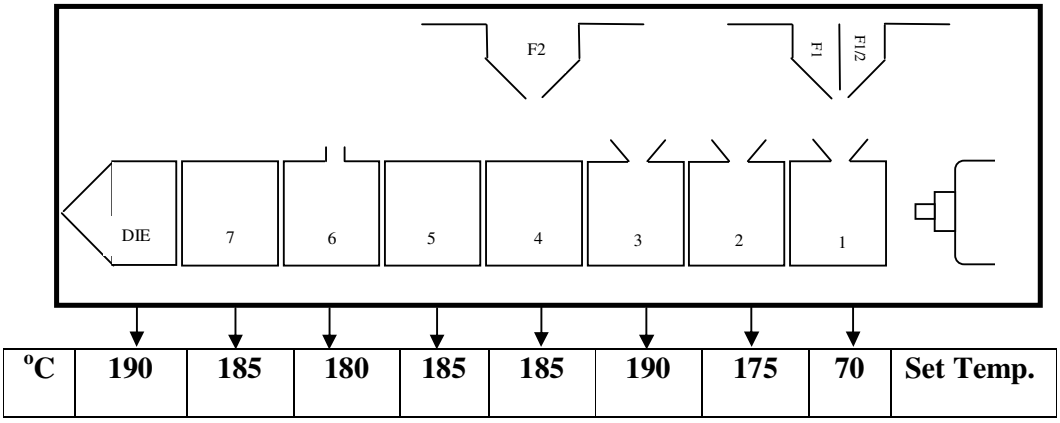

Figure 3.5. The schematical representation of set barrel temparature profiles.

Moreover, polypropylene nanocomposites with different combinations of organoclay, corresponding compatibilizer (i.e., PP-g-MA or EPDM-g-MA) and PP matrix were prepared as follows. Before the melt processing, all the components were dried at 80°C in oven at least for 12 h. Then, the granules or pelletes of PP and corresponding compatibilizer were dry-mixed and fed into the extruder through one feeder together,

while the organoclay was added through the other feeder. Furthermore, the polymer pellets and organoclay were metered independently in the required proportions with gravimetric dosing units in extruder.

The maleic anhydride grafted compatibilizer amount was three times higher than the organoclay by weight in preparing well-mixed polypropylene nanocomposites (PPNCs) in twin-screw extruder as Okada and co-workers [30, 31] referred in literature. For comparison, blends of PP and corresponding compatibilizer without organoclay and conversely, blends of PP and organoclay only without any compatibilizer were also compounded as control materials. A complete description of the blends of PP and the nanocomposites prepared in twin-screw extruder in this study is all given in Table 3.5.

Table 3.5. Description and composition of the PP blends and PP nanocomposites

Designation	**PP (wt %)**	**Compatibilizer type**	**Compatibilizer (wt %)**	**Organoclay (wt %)**
PP	100	-	-	-
PP/N3	97	-	-	3
PP/N5	95	-	-	5
PP/QF9/N3	88	QF-300 E	9	3
PP/QF15/N5	80	QF-300 E	15	5
PP/QF21/N7	72	QF-300 E	21	7
PP/QF9	91	QF-300 E	9	-
PP/M9/N3	88	M 613-05	9	3
PP/M15/N5	80	M 613-05	15	5
PP/M21/N7	72	M 613-05	21	7
PP/M9	91	M 613-05	9	-
PP/E3/N3	94	EPDM-g-MA	3	3
PP/E6/N3	91	EPDM-g-MA	6	3
PP/E9/N3	88	EPDM-g-MA	9	3
PP/E5/N5	90	EPDM-g-MA	5	5
PP/E10/N5	85	EPDM-g-MA	10	5
PP/E15/N5	80	EPDM-g-MA	15	5
PP/E21/N7	72	EPDM-g-MA-	21	7
PP/E9	91	EPDM-g-MA	9	-

In the designation of the samples, “PP” identifies polypropylene matrix, “QF” identifies QF-300 E (ADMER) which is one of the maleic anhydride grafted polypropylene (PP-g-MA) compatibilizer with high molecular weight (as a consequence of its low MFI value) and low maleic anhydride (MA) grafting content, “M” identifies M 613-05 (FUSABOND) which is the other PP-g-MA compatibilizer with low molecular weight (deduced from its high MFI value) and high MA grafting content. In addition, “E” stands for EPDM-g-MA coupling agent; whereas “N” denotes the nanoscale organoclay Nanofil-15. The numbers after the letters refer to the % weight fraction of the loading.

In general, with a given specifications of abovementioned compatibilizers it was thought that PP-g-MAs would work from tensile properties point of view, while EPDM-g-MA would work from impact properties of view. As a result, pale-yellow and/or pale-brown strands of the PPNCs were obtained. The strands that were obtained were cooled in a water bath, pelletized with a cutter and dried under vacuum at 80 ^{o}C. Then, the dried pellets of the PPNCs were injection molded into test specimen.

3.3.1. Twin-Screw Extruder and Process Parameters

In this work, an intermeshing co-rotating twin-screw extruder was used to manufacture the nanocomposite materials by melt mixing method. The modular twin screw extruder used was PRISM TSE 24 HC (see Figure 3.6), with 24 mm screw diameter (D) and 28:1 L/D ratio (shaft length over screw diameter). Some useful properties according to the producer’s (Thermo Electron Corporations) product specifications were given in Table 3.6.

Table 3.6. Technical specifications of Prism TSE 24 HC 28:1 extruder

PRISM TSE 24 HC 28:1	Units	Values
Barrel bore diameter	mm	24
Screw diameter	mm	23.6
Channel depth	mm	5.15
Max. screw speed	rpm	1000
Power at max. screw speed	kW	9.0
Max. torque/shaft	Nm	43
Barrel zones	Qty.	7
Extruder dimensions (L x W x H)	cm	165 x 60 x 135

PRISM TSE 24 HC extruder had 7 modular barrel segments, each were heat controlled and had a length of 4D (i.e., 24x4=96 mm). Barrel profiles were illustrated in Figure 3.7. Set temperatures were controlled by electrical resistances and water cooling channels, the 3rd, 5th and 7th barrels had thermocouples mounted to measure the melt temperature of the mixture inside the barrels.

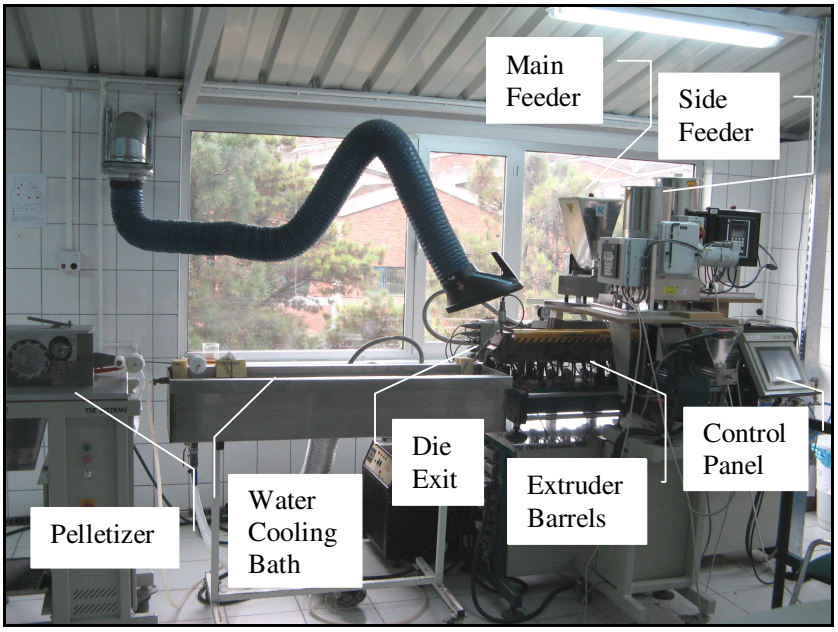

Figure 3.6. PRISM TSE 24 HC modular intermeshing co-rotating twin-screw extruder

The first barrel was called inlet zone, polymeric materials were fed from here and conveyed through the barrels by the effect of torque applied by the extruder screws. At the 6th barrel, there was a degassing unit connected. Gases occurring during the process were removed from here by a vacuum pump. The barrels end with a three-strand hole die and each hole was 3 mm in diameter. The die was mounted at the forward end of extruder, where the molten mixture can go out of the barrels as spaghetti shaped strands. Melt pressure generated by the movement of screws was measured by a pressure sensor connected to the die barrel.

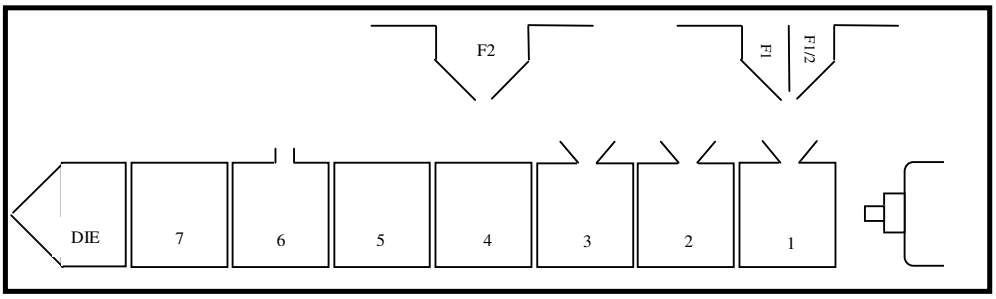

Figure 3.7. Barrel profile

Spaghetti shaped material was cooled down in a water bath (at ambient temperature). Then, these spaghettis were cut into small pieces (i.e., granules) by the pelletizer shown in Figure 3.8.

Figure 3.8. Pelletizer

The barrels of the extruder can be split horizontally in the middle for easy screw removal and cleaning purpose as shown in Figure 3.9.

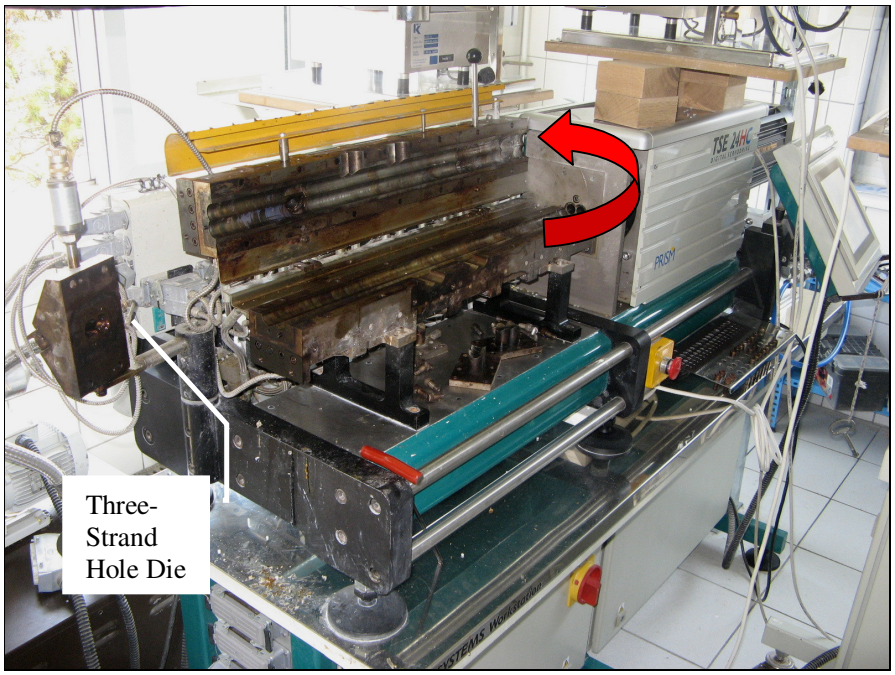

Figure 3.9. Extruder barrel splitted horizontally

The extruder was equipped with 3 feeders. Two of them were K-Tron gravimetric feeders and they were controlled with their own software program. The other was Brabender side feeder and was operated by PRISM controller system.

3.3.2. Injection Molding Machine and Process Parameters

In this work, Arburg Allrounder 320C Injection Molding Machine (Figure 3.10) was used to produce mechanical test specimens: tensile test specimens, and izod impact test specimens. Flexural tests were done by using impact test specimens. Some useful properties according to the producer's (Arburg) product specifications were given below in Table 3.7.

Table 3.7. Arburg Allrounder 320 C Injection Molding Machine technical specifications

Arburg Allrounder 320 C	Units	Values
Screw diameter	mm	30
Max. injection pressure	bar	2500
Drive power of the hydraulic pump	kW	15
Max. clamping force	kN	500

Injection molding process is defined as a process where molten plastic is injected at high pressure into a mold cavity. It takes its shape by cooling and solidifying in the mold. Injection Molding Machines consist of 3 main parts: Clamping unit keeps molten material under pressure during injection or cooling; injection unit consists of hopper, cylinder and screw; and finally mold is the part where the material cools down and takes its shape.

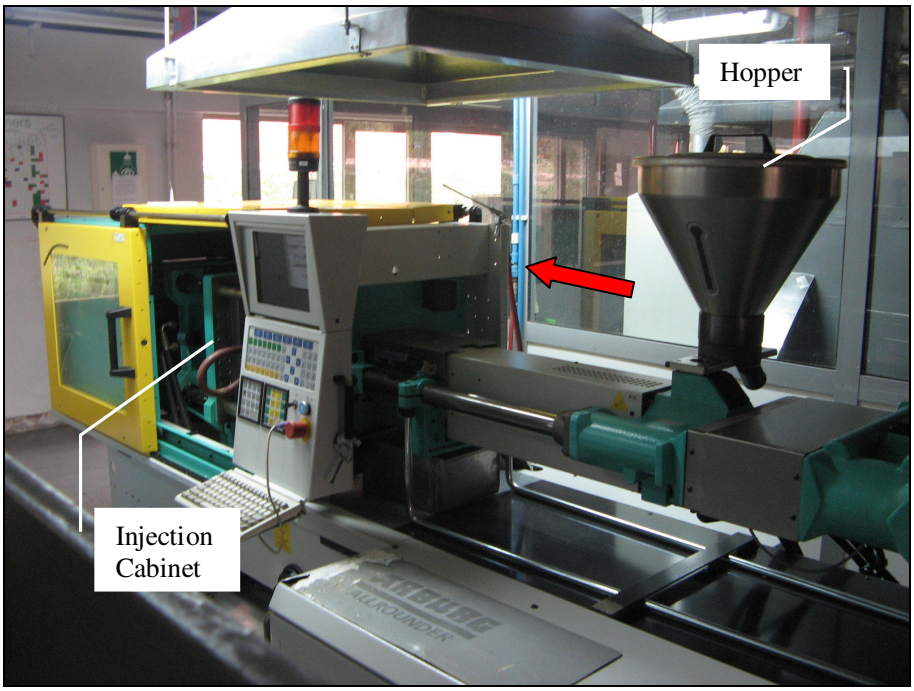

Figure 3.10. Arburg Allrounder 320 C Injection Molding Machine

Injection molding machine was fed by granule shaped nanocomposites. These granules were melted by heat through the screw. When the molten material came out the screw, injection began and the material was forced into the mold cavity by the movement of the screw. The screw held the force for a short period to compensate for the shrinkage

of the material. After the injection and holding the pressure, the mold was kept closed for cooling down. The material solidified, took its shape and then forced out of the mold by ejectors. Excessive parts of the product, such as runners and gates of the cavity, were cut by a belt saw, Rexon.

While manufacturing the test specimens for examining the mechanical properties of the nanocomposites, three types of molds were used to produce three types of samples. Normal tensile mold for tensile testing; weld-line tensile mold for weld-line tensile testing and impact mold for both flexural and impact testing (Figure 3.11). The shape and the dimensions of the weld-line tensile test specimen were same as the normal tensile one; however, the former was fed from two points into the cavity, so molten polymeric material met in the middle of the specimen creating a possible failure zone.

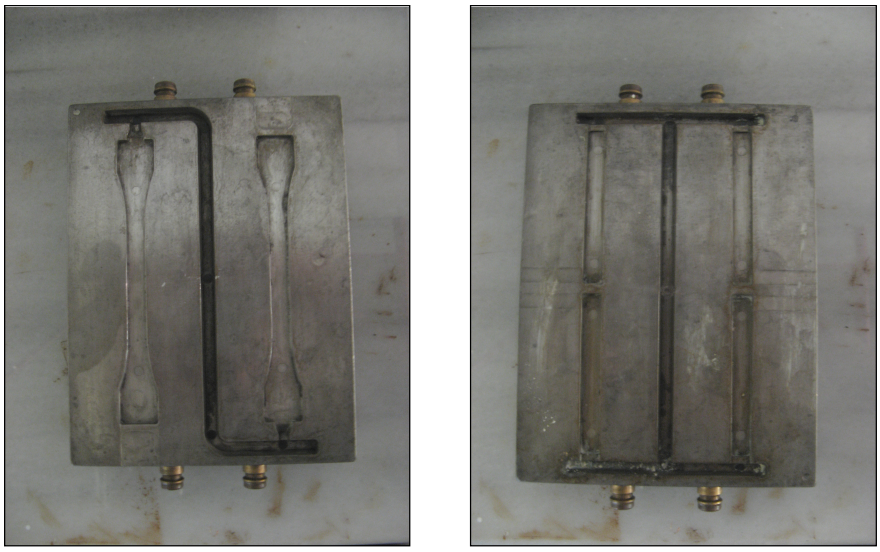

(a) Tensile test specimen (ISO R527)

(b) Flexural and impact test specimen (ISO 178, ISO180)

Figure 3.11. Molds designed for test specimens, (a) Tensile test specimen (ISO R527), (b) Flexural and impact test specimen (ISO 178, ISO180)

Time and pressure values of the three steps of injection and holding processes for the test specimens were shown in Table 3.8. Injections parameters were also given below.

Table 3.8. Injection and holding process parameters of Injection Molding Machine

Normal Tensile Test Specimen	**Unit**	**1st Step**	**2nd Step**	**3rd Step**
Injection Speed	cm^3/sec	120	125	110
Injection Pressure	bar	750	800	750
Holding Time	sec	0.2	5	3
Holding Pressure	bar	750	700	500
Shot Volume	cm^3	36		
Screw Speed	rpm	140		
Backpressure	bar	25		
Flexural and Impact Test Specimen	**Unit**	**1st Step**	**2nd Step**	**3rd Step**
Injection Speed	cm^3/sec	110	140	120
Injection Pressure	bar	850	1000	900
Holding Time	sec	0.2	5	3
Holding Pressure	bar	850	800	675
Shot Volume	cm^3	37		
Screw Speed	rpm	140		
Backpressure	bar	25		

3.4. Characterization and Testing of PP Nanocomposites

Nanocomposite materials which were melt compounded in twin screw extruder were tested for physical and mechanical properties using various procedures.

3.4.1. Structural Characterisation (XRD)

X-ray diffraction was done at small angles to determine the degree of clay intercalation and at wide angles to characterize the PP crystalline phases.. X-ray diffraction (XRD) measurements conducted on A Rigaku-D/Max-2200 Ultima+ Diffractometer (Rigaku, Tokyo, Japan) with CuK_α radiation ($\lambda = 1,54$ ^oA) operating at 40 kV and 40 Ma. The diffraction patterns were recorded in the reflection mode over a 2θ range of 1,5 to 10^o

at a rate of 2^o/min; the measurements were taken at equal increments of $0{,}02^o$ and the interlayer spacing (d_{001}) was calculated using Bragg's equation : $n\lambda = 2d\sin\theta$, where λ is the wavelength. The characterisation of the structure by XRD was carried out for powdered samples from pellets.

3.4.2. Thermal Stability Characterisation (TGA)

The thermal stability of the samples was characterized with a thermogravimetric analyzer (TGA) on TGA-Q50 (TA Instruments, New Castle, DE, USA) under nitrogen (inert atmosphere) flow. The heating process was conducted from room temperature to 600 °C at a rate of 10 °C/min.

3.4.3. Dynamic Mechanical Characterisation (DMA)

The dynamic mechanical properties of the nanocomposites were measured with a dynamic mechanical analyzer (DMA-Q800, TA Instruments, New Castle, DE, USA) in the single-cantilever mode at a frequency of 1Hz and a heating rate of 5 $^oC\ min^{-1}$ over a temperature range of -70 to 130 ^oC. The average dimensions of the injected samples were (*t* x *w* x *l)* 3 x 10 x 34 mm^3.

3.4.4. Static Mechanical Characterisation

Injection molded test specimens were kept in air conditioned room for at least 48 hours to eliminate the effects of residual stresses. Room temperature was fixed at 23 ± 2 $^{\circ}C$ and the relative humidity was 50%. The mechanical tests were also performed under these conditions.

Three types of mechanical tests were applied on the nanocomposites. Tensile, flexural and impact resistance properties were measured in these tests and were reported below.

3.4.4.1. Tensile Test. Tensile strength of the materials was measured by a Zwick Universal Tensile Testing Machine Z020 according to ISO R527 standard [47]. Load indicator equipment was a 20 kN load cell and extension indicator was a mechanical long stroke extensometer.

Test specimens were left at the air conditioned room (23 ± 2 ˚C and 50% relative humidity) for at least 48 hours, and then measured in thickness and width before testing to obtain the cross section area of the sample (Figure 3.12). Both tensile and weld-line tensile test specimens are 150 mm in length and 3 mm in thickness. Afterwards, the specimen was fixed to self-aligning grips of the tensile test machine with 123 mm distance between grips. The extensometer was attached to the specimen and the gauge distance of the extensometer was 700 mm. Test was performed at a constant speed of 50 mm/min and the stress and corresponding strain values were recorded at 0.1 second time intervals.

Following tensile properties were reported at the end of the test:

- Maximum stress [N/mm^2]
- Strain at maximum load [%]
- Stress at break [N/mm^2]
- Strain at break [%]
- Elastic Modulus (Young Modulus) [N/mm^2]
- Work up to maximum load [Nmm]

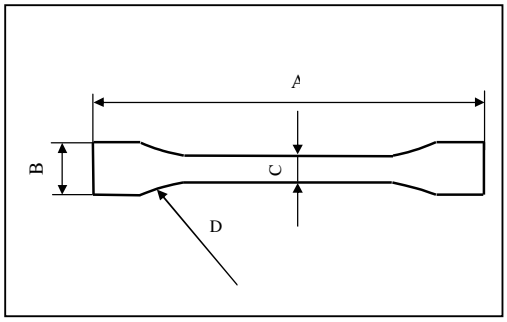

A Overall length, minimum:	150 mm
B Width at ends:	20±0.5 mm
C Width of narrow parallel portion:	10±0.5 mm
D Radius, minimum:	60 mm

Figure 3.12. Tensile test specimen according to ISO R527 [47]

3.4.4.2. Flexural Test. Flexural properties of the nanocomposite materials were measured by an Instron 4505 Universal Tensile Testing Machine according to ISO 178 [48]. Load indicator equipment was a 5 kN load cell. A three point bending fixture was used for testing.

Izod impact test specimens were used for flexural testing. Considering ISO 178 standards, specimens were 80±0.5 mm in length (L), 10±0.5 mm in width (w) and 4±0.2 mm in thickness (t) as shown in Figure 3.13. All the test specimens were measured by a micrometer with 0.02 mm sensitivity before testing to obtain the cross section area. These specimens were tested after a 48 hours from injection molding. They were left in an air conditioned room for 48 hours at 23±2 ˚C and with 50% relative humidity. Flexural test was also performed at these conditions.

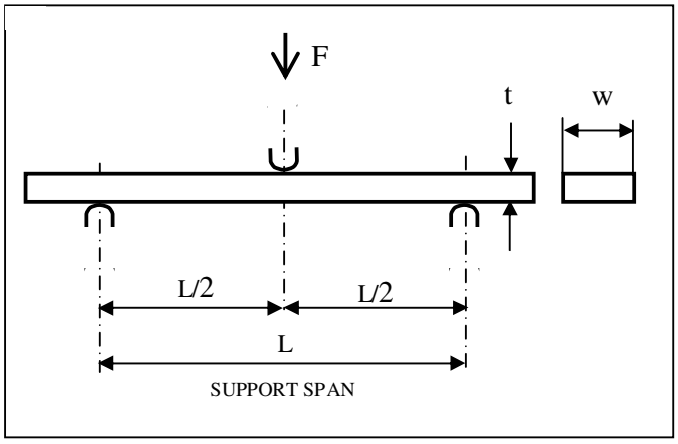

Figure 3.13. Flexural test specimen loaded in three point bending

The specimen was put on the lower arm of the bending fixture connected to the stationary testing machine base. The upper arm of the fixture which was connected to the movable crosshead of the testing machine was slowly contacted with the test specimen at mid-span and the test was started. Test was performed at a constant crosshead speed of 5 mm/min and the load and corresponding extension values were measured by travel distance of the movable part and they were recorded in a 0.2 second time interval.

Following flexural properties were reported at the end of the test:

- Stress at yield [N/mm^2]
- Strain at yield [%]
- Elastic Modulus (Young Modulus) [N/mm^2]

3.4.4.3. Impact Test. Izod impact strength of the test materials was measured by a Zwick Impact Tester which tests up to 2.75 Joules by the versatile impact pendulum according to ISO 180 standard [49].

Injection molded test specimens were left for 48 hours to eliminate the effects of post crystallization and then tested in an air conditioned room (with a temperature 23±2 ˚C and with 50% relative humidity). Specimen dimensions were 80±0.5 mm in length, 10±0.5 mm in width and 4±0.2 mm in thickness considering ISO 180 standard. All the test specimens were measured by a micrometer with 0.02 mm sensitivity before testing to

obtain the cross section area. Afterwards, 2 mm notch (v-shaped) was machined at mid-span of specimen. A test without a specimen was done to confirm the frictional loss which is 0.038 J. Then the specimen was placed into the grips of the testing machine and the pendulum was released. The notched surface should be faced to the impact point (see Figure 3.14).

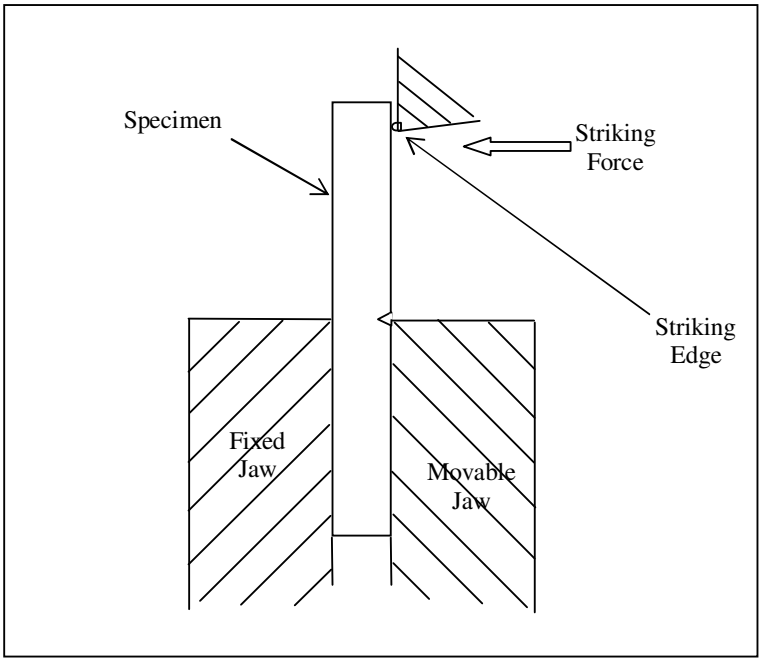

Figure 3.14. Izod Impact test set-up

The impact energy was measured and by the addition of frictional loss, the correct impact energy [J] was calculated. The Izod impact strength [kJ/m^2] was calculated by the dividing the impact energy to the cross-section area of the sample.

3.4.5. Morphological Characterisation (ESEM)

The morphology of the samples was examined using Philips XL-30 scanning electron microscpe. The samples were cryogenically fractured in liquid nitrogen and the fracture surfaces of the composites were observed without any requirement of coating in an ESEM-FEG/EDAX Philips XL-30 (Philips, Eindhoven, The Netherlands) instrument

using an accelerating voltage of 10 kV, which could show the dispersion of the filler in the matrix. In addition, PPNCs containing EPDM-g-MA was etched in *n*-heptane at 50 ^{o}C for 3 h to extract the elactomeric phase. Magnification of 5000X and 10000X were used

3.4.6. Atomic Force Microscopy (AFM)

Atomic Force Microscopy (AFM) was performed using Quesant-Ambios Universal Scanning Probe Microscope (USPM) (Ambios Technology, Santa Cruz, CA). Hot pressed thin films were directly scanned for investigating dispersion of rubber particles (in case of PPNCs containing MA grafted elastomeric compatibilizers) and organoclay phase in PP matrix. Phase mode imaging was performed using a silicon nitride cantilever probe with a nominal resonance frequency around 170 kHz and a nominal tip radius of 5-10 nm.

4. RESULTS AND DISCUSSION

The composites of organoclay and various compatibilizers prepared in the lab-scale internal mixer in hope of finding guidelines for the suitable loading of organoclay and compatibilizers in PP nanocomposites were then prepared on a twin-screw extruder. The exfoliation or intercalation behavior of PP nanocomposites was examined at various loadings for the three types of compatibilizers. MA-functionalized compatibilizers have been used for preparing PP nanocomposites [15]. According to a literature review, the exfoliation/intercalation of layered silicates is generally enhanced by the loading of compatibilizer being increased. However, there are many differences in the characteristics of the compatibilizers such as various molecular weights and MA contents reported in the literature. On the other hand, the exfoliation/intercalation power of the compatibilizers could be realized at a weight ratio (compatibilizer to organocaly) of roughly 3, regardless of the differences in the compatibilizers. Therefore, weight ratios around that value were selected for the following formulations.

4.1. Combined Effects of PP-g-MA Compatibilizers with Different Characteristics and Organoclay Loading on the Formulation and Physical, Thermal, and Mechanical Properties of PPNCs

In order to evaluate the role of organoclay content and PP-g-MA compatibilizer addition on nanocomposite structure, morphology, and mechanical properties, commercially available Org-MMT was melt-mixed with PP matrix and different PP-g-MA compatibilizers

4.1.1. Structural Characterization (XRD)

XRD is a rather simple and widely employed technique for the characterization of clay dispersibility. The level of intercalation in PP nanocomposites was determined by the

measurement of the clay interlayer spacing (d_{001}) from the 2θ position of the clay (001) diffraction peak using Bragg's law. X-ray parameters of corresponding PP blends and PP nanocomposites, namely; 2θ and *d*-spacing (in nm) values, calculated from the (001) peaks are summarized in Table 4.1.

Table 4.1. XRD parameters of PP blends and PP nanocomposites

Code	**Designation**	**PP Blends/Nanocomposites**	**2θ (°)**	***d*-spacing (nm)**
PPCC1	PP/N3	PP+Nano-15(3%)-uncompatibilized sys.	3,401	2,60
PPCC2	PP/N5	PP+Nano-15(5%)-uncompatibilized sys.	3,466	2,55
PPNC1	PP/QF9/N3	PP+QF-300 E(9%) [PP-g-MA]+Nano-15(3%)	2,978	2,96
PPNC2	PP/QF15/N5	PP+QF-300 E(15%) [PP-g-MA]+Nano-15(5%)	2,803	3,15
PPNC3	PP/QF21/N7	PP+QF-300 E(21%) [PP-g-MA]+Nano-15(7%)	3,069	2,88
PPNC4	PP/M9/N3	PP+M 613-05(9%) [PP-g-MA]+Nano-15(3%)	3,132	2,82
PPNC5	PP/M15/N5	PP+M 613-05(15%) [PP-g-MA]+Nano-15(5%)	2,972	2,97
PPNC6	PP/M21/N7	PP+M 613-05(21%) [PP-g-MA]+Nano-15(7%)	3,069	2,88

The interlayer spacing of organoclay used is 2,93 nm before compounding. As it can be seen in Table 4.1, for the uncompatibilized systems, the XRD patterns exhibited a significant decrease in interlayer spacing to 2.60 and 2,55 nm after mixing. This indicates that the polypropylene does not intercalate into the interlayer, even if the montmorillonite is modified with dimethyl dihydrogenated tallow ammonium ions. That is, there is a collapse in the clay galleries in compatibilizer-free composites. Therefore, to improve the intercalation and dispersion of the clay in nanocomposites, usage of maleic anhydride modified PP oligomers with the larger compatibility to PP matrix such as PP-g-MA seems to be essential.

Figure 4.1 and 4.2 show the XRD patterns of organoclay and PPNCs with QF-300 E and M 613-05. QF-300 E has a high molecular weight, as a result of low MFI value, and low MA content, whereas M 613-05 has a low molecular weight, as a result of high MFI value, and high MA content, respectively.

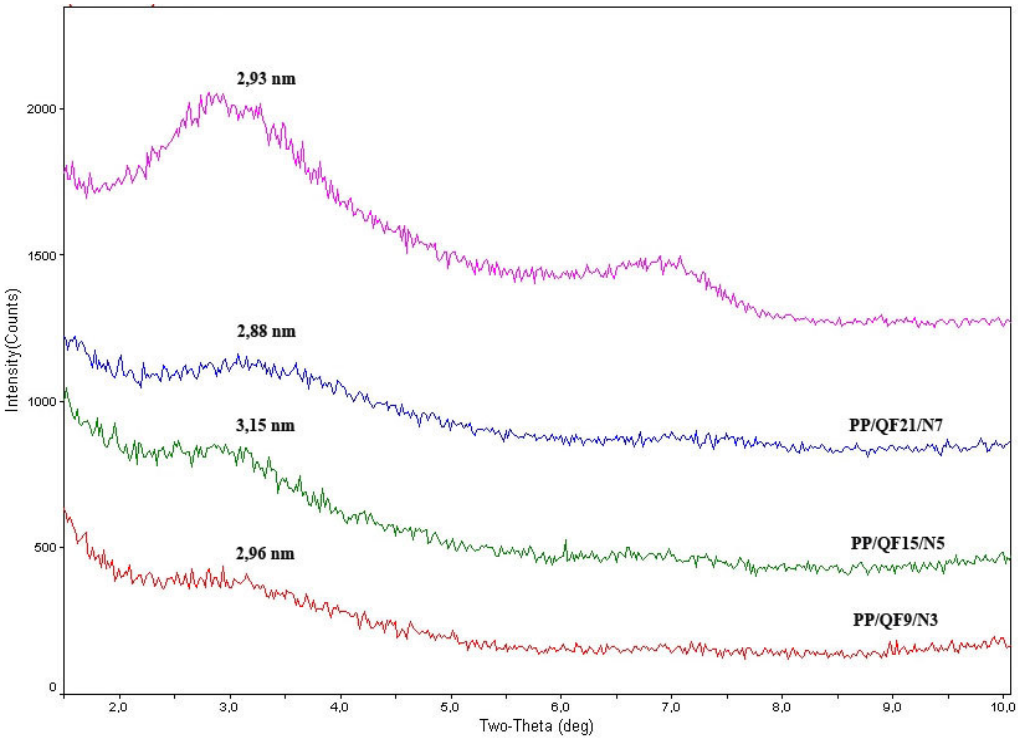

Figure 4.1. XRD patterns of organoclay and PPNCs with QF-300 E

As can be seen from Figure 4.1, especially, in the PP/QF9/N3 and PP/QF15/N5 nanocomposites in which QF-300 E used as PP-g-MA compatibilizer, the (001) organoclay plane peak of around 2θ = 3,010° were shifted to lower angles at about 2θ = 2,978° and 2,803°, respectively; comparable to that of organoclay, implying that the interlayer distance was increased from 2,93 nm to 2,96 and 3,05 nm, respectively; during the direct melt blending process. This clearly indicates that the macromolecule chains had intercalated into the galleries of organoclay.

On the other hand, in PP/QF21/N7 nanocomposite, the peak position moved toward a very slightly higher angle of about 3,069° compared to organoclay plane peak which is at 3,010°. As a consequence of this, the organoclay interlayer distance in PP/QF21/N7

decreased a little bit to 2,88 nm. This smaller basal-spacing with respect to organoclay indicates that a collapse in the clay sheets most probably due to a microphase separation resulted from high concentrations of graft copolymer.

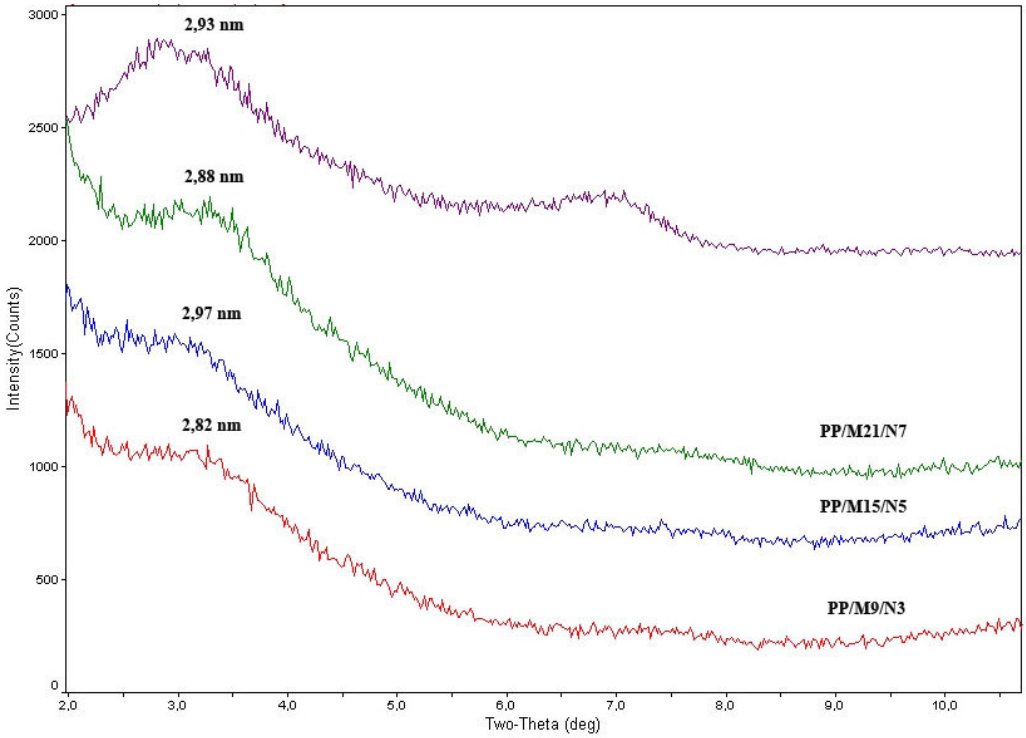

Figure 4.2. XRD patterns of organoclay and PPNCs with M 613-05

In the case of PPNCs containing M 613-05 as a PP-g-MA compatibilizer, the characteristic (001) plane diffraction peak of organoclay (2θ = 3,010° with *d*-spacing = 2,93 nm) shifted to a lower angle of 2θ = 2,972° with the corresponding *d*-spacing of 2,97 nm only in PP/M15/N5 nanocomposite. This shifting denoted the expansion of organoclay interlayer spacing, which is attributed mostly to intercalation of PP-g-MA inside the organoclay galleries.

However, the decreased interlayer distance of PP/M9/N3 and PP/M21/N7 nanocomposites (2,82 and 2,88 nm, respectively), compared with that of organoclay (2,93 nm), provides an estimation on the chain conformation of PP-g-MA intercalated between the layers; that is, PP-g-MA chains, perhaps, run parallel to the interlayers with an extended conformation. Therefore, the decreased interlayer distance of organoclay after

compounding with PP-g-MA may be explained the by lack of the possibility of a chemical reaction between organoclay and PP-g-MA (M 613-05) in such conformation.

It is quite clear that when PP and organoclay were blended, no increase, even a significant decrease, of the interlayer spacing of the organoclay was observed, as tabulated in Table 4.1. Therefore, according to XRD results of PP nanocomposites containing all three components, only PP-g-MA can intercalate into the silicate layers during the melt-mixing process. The increasing of interlayer distance of organoclay in intercalated PP nanocomposites may be the result of the strong interaction between polar PP-g-MA conpatibilizer and the silicate layer. The driving forces of the intercalation originate from the strong hydrogen bonding between MA group (COOH group generated from the hydrolysis of the MA group) and the oxygen groups of the silicates. As a result, the interlayer spacing of the clay increases and the interaction of the layers weaken. The intercalated clay with the compatibilizer contacts with PP under a strong shear field during extrusion process and this leads macromolecule PP chains intercalated into the galleries of organoclay. If the miscibility of PP-g-MA with PP is good enough to disperse at the molecular level, the exfoliation of the intercalated clay should take place smoothly. On the other hand, if the miscibility is not good enough, the phase separation occurs with no exfoliation. Therefore, it is quite reasonable to say not only the intercalation ability of the oligomers but also the miscibility should be a very important factor to achieve the exfoliated homogeneous dispersion of the clays in this novel approach using oligomers as a compatibilizer.

Kim et al.[50] reported that, when the three components of PP, PP-g-MA, and organoclay were put together and melt mixed, only PP-g-MA would penetrate into the organoclay interlayer. Once the functionalized polymers are intercalated into the gallery, they constitute the long-chained surfactants. The matrix polymer can then readily penetrate into the thick interlayer and form a broad interphase, which results in the formation of intercalated/exfoliated structure.

From the results of XRD analysis, scenarios for the mechanisms of clay dispersion and intercalation in the presence of the two compatibilizers can be proposed. The schematic representation of these proposed scenorios are shown in Figure 4.3.

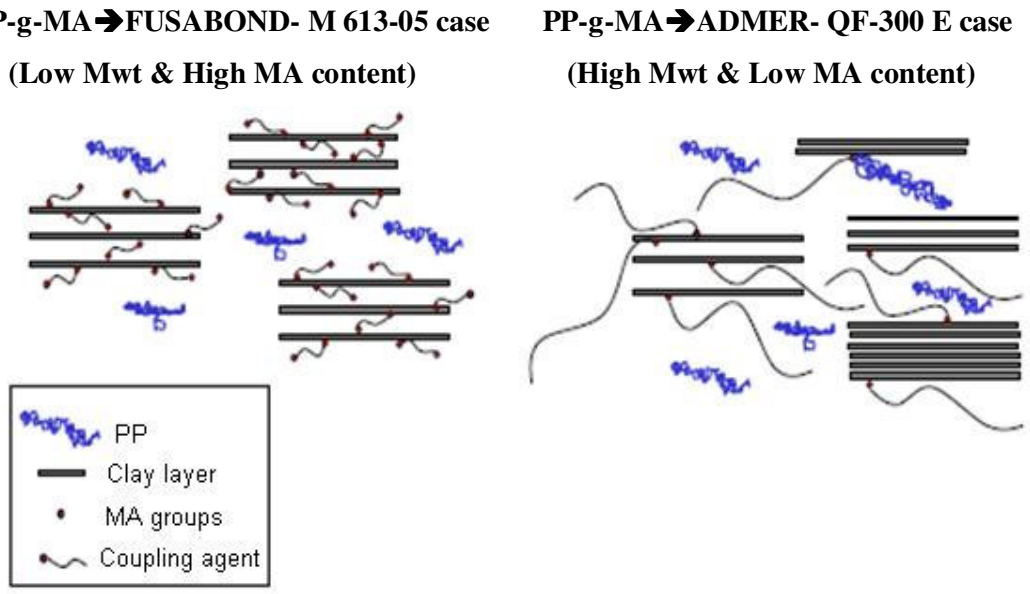

Figure 4.3. Schematic representation of clay intercalation process with the two different MA grafted PP compatibilizers [51]

When a coupling agent with a low molecular weight (deduced from its high MFI value) is used, such as Fusabond-M 613-05, the *high mobility* of its short chains and their relatively high grafting content allow them to interact actively with a large number of clay platelets and a high clay surface area during compounding. This leads to good clay dispersion in PP/M15/N5. However, even though the high MA content of M 613-05 seems to lead to high compatibility with the clay, its low molecular weight reduces its compatibility with the PP matrix in terms of co-crystallization. Recall that in a crystalline system, maximum compatibility between the coupling agent and the matrix can only be obtained if *co-crystallization* occurs. So, this incompatibility probably explains the slight collapseof the clay platelets in PP/M9/N3 and PP/M21/N7 nanocomposites. Moreover, when compared to uncompatibilized systems, the relative uniformity of the intercalation process in PP/M15/N5 suggests that only M 613-05 molecules penetrate between the

platelets, otherwise larger degree of intercalation and larger interlayer spacing would not be obtained. As a consequence, the platelets distance is limited by the length, and perhaps, orientation of the chains of M 613-05. Effective intercalation can thus be obtained, but it cannot be enhanced to high clay interlayer spacing.

When a coupling agent with a high molecular weight (deduced from its low MFI value) is used, such as Admer-QF-300 E, the *low mobility* of its long chains and their relatively low grafting content allow them to interact with a limited number of clay platelets and a low level of clay surface area. This leads to good clay dispersion in PP/QF9/N3 and PP/QF15/N5 nanocomposites but a less effective intercalation process in PP/QF21/N7. Because of the long chains of QF-300 E and its expected better miscibility with the PP matrix that can accommodate for further larger intercalation, the intercalation of this coupling agent leads to a more effective and larger platelets distancing as seen by higher clay interlayer spacing, especially in PP/QF15/N5. Moreover, it favors a better and finer dispersion. Besides, due to the characteristics of this coupling agent as the low MA grafting content, limited intercalation still remains. Different extent of intercalation is thus obtained with QF-300 E, some with higher level compared to M 613-05 but as a consequence, in all cases, the existence of a diffraction peak clearly indicates the partly intercalated and stacked structures.

4.1.2. Thermal Characterization (TGA)

The thermal stability of the nanocomposites has been examined by using TGA; the parameters for the PP nanocomposites are shown in Table 4.2 and include the temperature at which 10% degradation occurs, almost a measure of the onset temperature of degradation (the temperature at which degradation begins), the temperature at which 50% degradation occurs, the midpoint of the degradation process, and the fraction of material which remains at 600 ^{o}C, denoted as *char* (non-volatile residue). Table 4.2 reveals that regardless of the kind of the PP-g-MA compatibilizers used, all PP nanocomposites showed enhanced thermal stability.

Table 4.2. Thermal Properties of neat PP, PP Blends, and PP Nanocomposites

Designation	PP Nanocomposites/Blends	$T_{-10\%}$ (^{o}C)	$T_{-50\%}$ (^{o}C)	Char at 600 ^{o}C (%)
PP	PP-Homopolymer-Borealis 125 MO	344,13	390,50	0,9160
PP/N3	PP+Nano-15(3%)-uncompatibilized sys.	401,37	424,50	2,743
PP/N5	PP+Nano-15(5%)-uncompatibilized sys.	412,68	429,82	3,807
PP/QF9/N3	PP+QF-300E(9%)[PP-g-MA]+Nano-15(3%)	431,12	438,90	1,980
PP/QF15/N5	PP+QF-300E(15%)[PP-g-MA]+Nano-15(5%)	424,69	436,37	3,645
PP/QF21/N7	PP+QF-300E(21%)[PP-g-MA]+Nano-15(7%)	424,34	444,20	5,037
PP/QF9	PP+QF-300E(9%)[PP-g-MA]-BLANK	385,52	443,34	0,4807
PP/M9/N3	PP+M613-05(9%)[PP-g-MA]+Nano-15(3%)	424,70	438,02	2,202
PP/M15/N5	PP+M613-05(15%)[PP-g-MA]+Nano-15(5%)	431,56	442,03	3,137
PP/M21/N7	PP+M613-05(21%)[PP-g-MA]+Nano-15(7%)	428,27	441,60	4,450
PP/M9	PP+M613-05(9%)[PP-g-MA]-BLANK	426,33	455,36	0,1637

The TGA curves, in nitrogen atmosphere, showed a single degradation step for all samples.. Figure 4.4 and 4.5 show the TGA curves of PP nanocomposites containing QF-300 E and M 613-05 as PP-g-MA compatibilizers, respectively. The onset degradation temperature ($T_{-10\%}$) is about 80 ^{o}C higher for the PP nanocomposites containing either QF-300 E or M 613-05 PP-g-MA compatibilizers than for neat PP matrix. The changes in the temperature at which 50% degradation occur also parallel the changes in onset temperature. As seen in Figures 4.4 and 4.5, the thermal stability of PP nanocomposites is evidently better than that of pure PP and PP blends. That is, the TGA curves of PP nanocomposites containing all three components showed a drastic shift of weight loss towards higher temperature. The improvement in the thermal stability, may have resulted from the interaction between the organic and inorganic phases. Individual layers of intercalated clay platelets acted as insulators, and the formation of a tortuous path between

the layers also inhibited the passage of volatile degradation products and hence enhanced the thermal stability of the clay composites.

In addition, in Table 4.2, the char residue of nanocomposites tends to increase, compared with that of the polymer matrix. The char residue of pure PP is 0.9160 wt %, because the condition is under nitrogen, which leads to part of the polymer being carbonized.

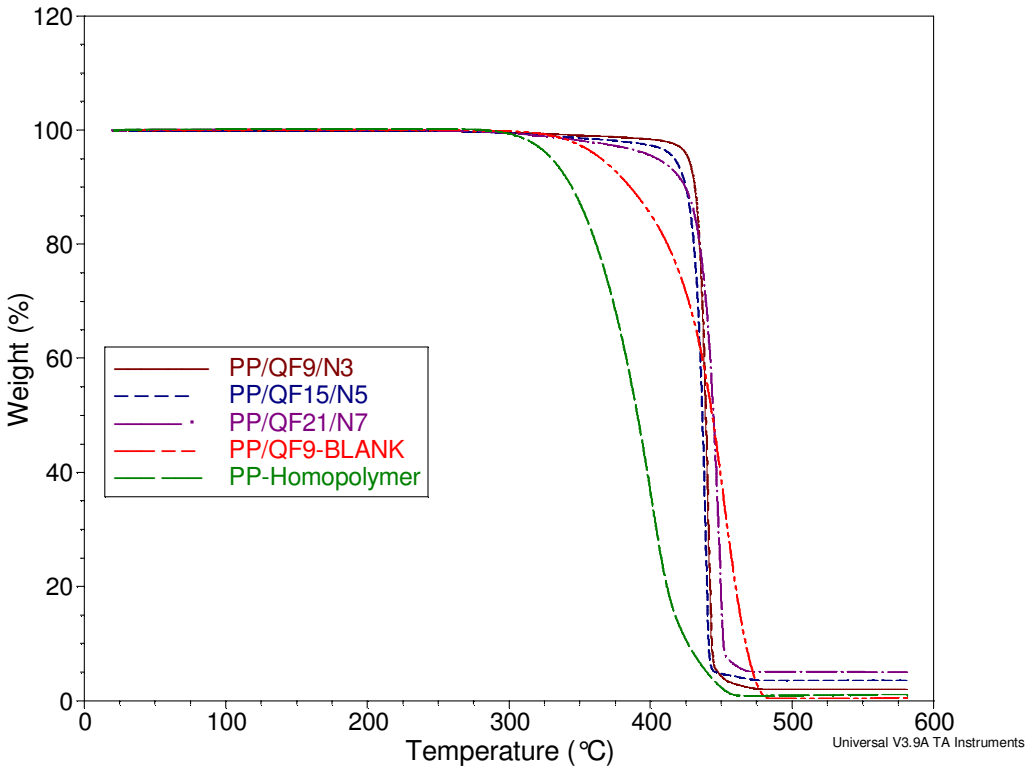

Figure 4.4. TGA thermograms of neat PP, PP/QF(9%)-Blank Blend and PP nanocomposites containing QF-300 E

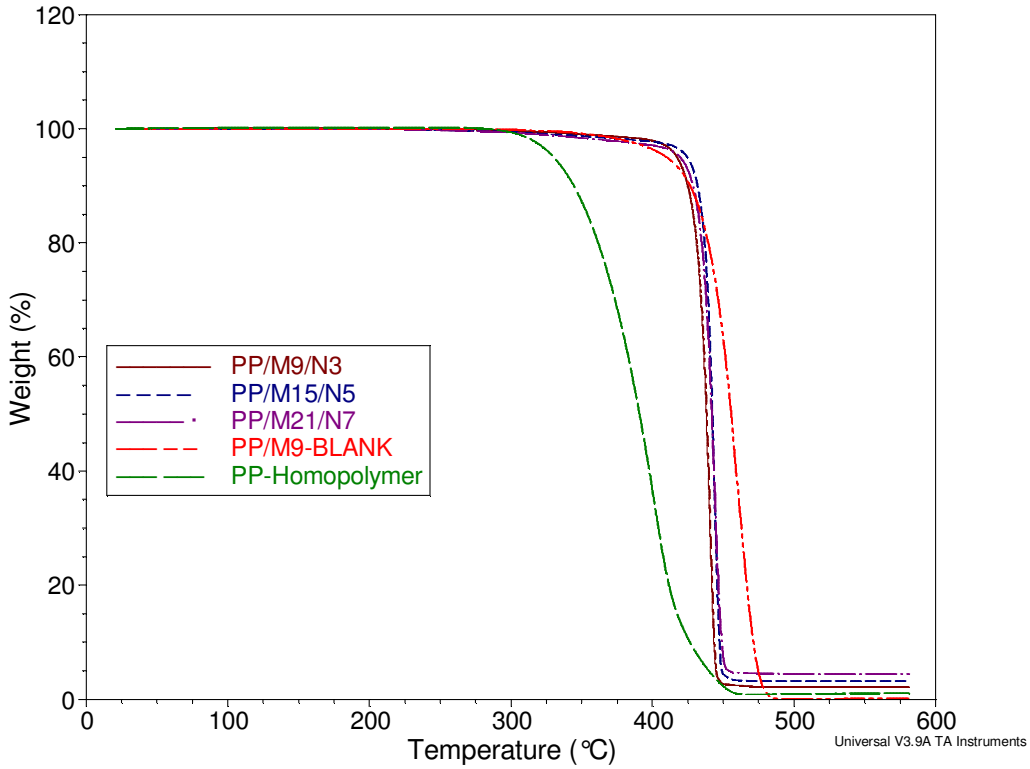

Figure 4.5. TGA thermograms of neat PP, PP/M(9%)-Blank Blend and PP nanocomposites containing M 613-05

4.1.3. Dynamic Mechanical Characterization (DMA)

The dynamic storage moduli (*E'*) spectra of the neat PP and PP nanocomposites containing QF-300 E and M 613-05 as PP-g-MA compatibilizers are given in Figure 4.6 and 4.7, respectively. The representative values of storage moduli (*E'*) at -50, 0, 30, 60, 100 ^{o}C were listed in Table 4.3. In order to clarify the effect of the layered silicates on the storage moduli (*E'*), the relative values of *E'* divided by neat PP value at each temperature were also given in paranthesis in the Table 4.3.

Table 4.3. Dynamic Storage Moduli of neat PP, PP Blends and PP nanocomposites with two types of PP-g-MA compatibilizers at Various Temperatures

Designation	PP Nanocomposites/Blends	-50 °C (MPa)	0 °C (MPa)	30 °C (MPa)	60 °C (MPa)	100 °C (MPa)
PP	PP-Homopolymer-Borealis HE 125 MO	3148 (-)	2531 (-)	1522 (-)	785,1 (-)	328,5 (-)
PP/N3	PP+Nano-15(3%)-uncompatibilized sys.	3686 (1,17)	2798 (1,11)	1612 (1,06)	850,9 (1,08)	375,5 (1,14)
PP/N5	PP+Nano-15(5%)-uncompatibilized sys.	3669 (1,17)	2789 (1,10)	1607 (1,06)	857,9 (1,09)	383,8 (1,17)
PP/QF9/N3	PP+QF-300 E(9%)[PP-g-MA]+ Nano-15(3%)	3695 (1,17)	2814 (1,11)	1680 (1,10)	903,9 (1,15)	394,9 (1,20)
PP/QF15/N5	PP+QF-300 E(15%)[PP-g-MA]+ Nano-15(5%)	3741 (1,19)	2822 (1,11)	1688 (1,11)	900,9 (1,15)	393,3 (1,20)
PP/QF21/N7	PP+QF-300 E(21%)[PP-g-MA]+ Nano-15(7%)	3507 (1,11)	3765 (1,49)	1669 (1,10)	872,6 (1,11)	382,4 (1,16)
PP/QF9	PP+ QF-300 E(9%)[PP-g-MA]-BLANK	3461 (1,10)	2591 (1,02)	1502 (0,99)	796,2 (1,01)	341,5 (1,04)
PP/M9/N3	PP+M 613-05(9%)[PP-g-MA]+ Nano-15(3%)	3819 (1,21)	2905 (1,15)	1674 (1,10)	885,7 (1,13)	421,4 (1,28)
PP/M15/N5	PP+M 613-05(15%)[PP-g-MA]+ Nano-15(5%)	3910 (1,24)	3004 (1,19)	1740 (1,14)	894,9 (1,14)	415,5 (1,26)
PP/M21/N7	PP+M 613-05(21%)[PP-g-MA]+ Nano-15(7%)	3804 (1,21)	2967 (1,17)	1769 (1,16)	840,3 (1,07)	388,4 (1,18)
PP/M9	PP+M 613-05(9%)[PP-g-MA]-BLANK	3407 (1,08)	2575 (1,02)	1392 (0,91)	707,5 (0,90)	330,4 (1,01)

*The values in each parenthesis represent the relative values of *E'* divided by neat PP value at each temperature

It is well-known that the storage modulus (*E'*) obtained through dynamic machanical analysis can provide useful information on the dynamic mechanical properties of the tested samples. Figure 4.6 and 4.7 represent *E'* as a function of temperature. As seen in both Figures, the examined samples exhibited a similar trend as *E'* decreasing with increasing temperature. This behavior is probably because of the increase in segmental polymer chain motion with temperature. Moreover, regardless of the kind of PP-g-MA compatibilizers used (whether QF-300 E or M 613-05), the dynamic storage moduli (*E'*) of the PP nanocomposites were higher than that of neat PP within the whole temperature range of the experiment, as seen in Figures. This storage modulus improvement is more pronounced in the early stages of the experiment; namely, at the low temperature range of the experiment, for both cases. That is to say, the enhancement of storage modulus (*E'*) is

evident in the lower temperature region (below T_g which is around 20 ^{o}C). As the temperature approaches to much higher temperatures, nearly to the melting point (T_m) of PP, the storage modulus (*E'*) values of the samples converged to a close value because of the softening effect.

In order to confirm the assumption that the reinforcement effect is attributed to the dispersed clays in the PP nanocomposites, the dynamic storage moduli of PP/QF(9 wt%) and PP/M(9 wt%), which are considered to be the blank blends, and those of the blends of PP with the organoclay (uncompatibilized sys.), the PP/N3 and the PP/N5, were measured and tabulated in Table 4.3. The dynamic moduli of PP/QF(9 wt%) and PP/M(9 wt%) exhibited lower values compared to those of PP at 30 ^{o}C (above *T*g), while those of the blends of PP with the organoclay exhibited slightly higher moduli. From these results, the enormous reinforcement effect observed in the PP nanocomposites should be attributed to the hybrid structures of them in which the silicate layers are dispersed far better than those in the blends of PP and the organoclay.

Furthermore, the significant enhancement of dynamic storage moduli (*E'*) observed for PP nanocomposites with appropriate PP-g-MA compatibilizer is believed to be due to the nanoscaled dispersion of layered silicates. This resulted in well-dispersed clay platelets which were already revealed in the XRD results. That is, since the dispersion of organoclay was good enough in PP nanocomposites designated as PP/QF15/N5 and PP/M15/N5, these nanocomposites show relatively much higher *E'*s than others.

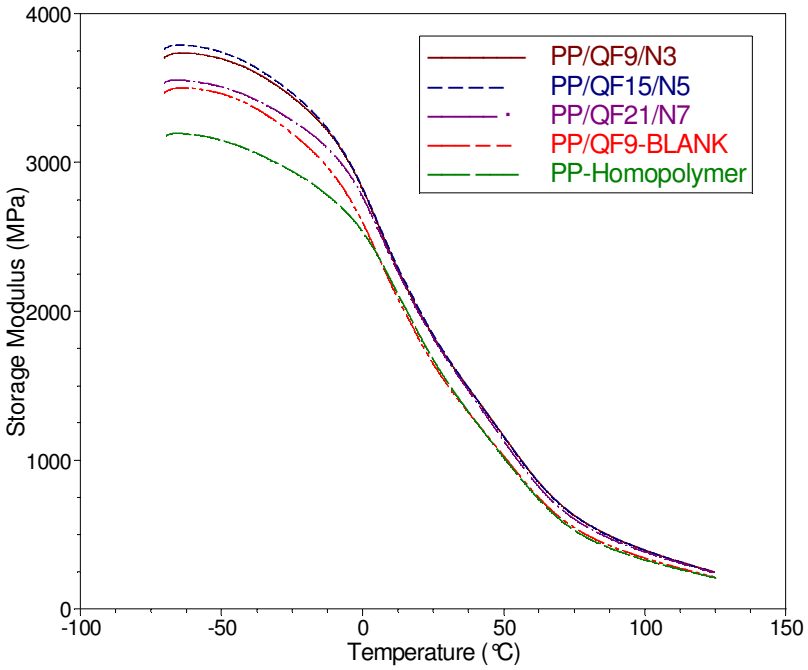

Figure 4.6. Dynamic storage moduli (*E'*) of neat PP, PP/QF(9 %) blank blend (organoclay-free) and PP nanocomposites containing QF-300 E

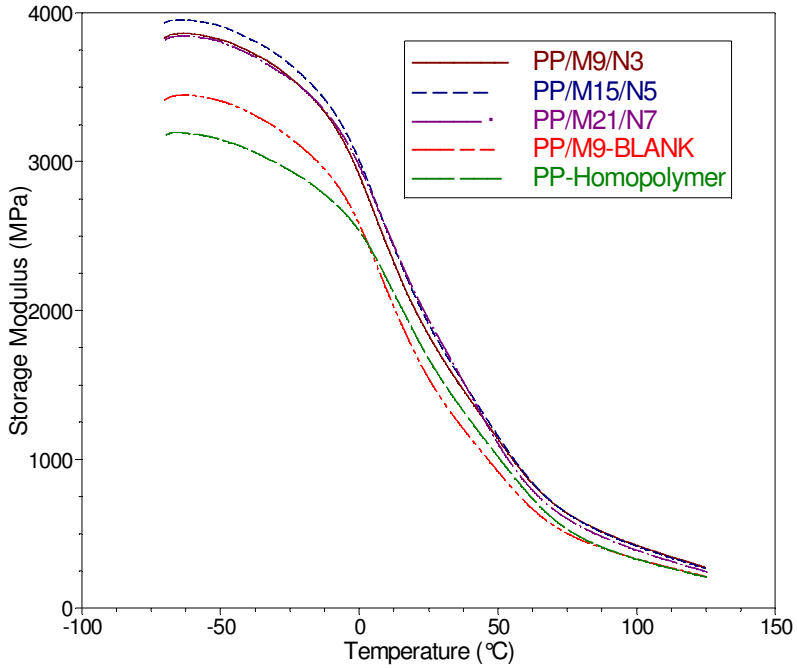

Figure 4.7. Dynamic storage moduli (*E'*) of neat PP, PP/M(9 %) blank blend (organoclay-free) and PP nanocomposites containing M 613-05

4.1.4. Static Mechanical Properties

The tensile and flexural properties of neat PP, PP blends and PP nanocomposites were measured and are summarized in Table 4.4. The effect of the organoclay content as well as compatibilizer on the tensile and flexural properties can be analysed using the results showed in that table. All prepared PP nanocomposites containing either QF-300 E or M 613-05 as PP-g-MA compatibilizer showed a significant improvement of Young's modulus with respect to neat PP and organoclay-free PP/Compatibilizer blank blends. Similar trend was observed for the flexural modulus of all nanocomposites.

Table 4.4. Mechanical Properties (tensile and flexural) of neat PP, PP blends and PP nanocomposites with two types of PP-g-MA compatibilizers at 25 ^{o}C

Designation	**PP Nanocomposites/Blends**	**Tensile Modulus (MPa)**	**Tensile Max. Stress (MPa)**	**Flexural Modulus (MPa)**	**Flexural Max. Stress (MPa)**
PP	PP-Homopolymer-Borealis HE 125 MO	1429,07	33,25	1298,75	38,84
PP/N3	PP+Nano-15(3%)-uncompatibilized sys.	1567,48	33,03	1280,13	41,91
PP/N5	PP+Nano-15(5%)-uncompatibilized sys.	1484,42	32,53	1255,18	40,19
PP/QF9/N3	PP+QF-300E(9%)[PP-g-MA]+Nano-15(3%)	1666,84	35,47	1509,24	43,59
PP/QF15/N5	PP+QF-300E(15%)[PP-g-MA]+Nano-15(5%)	1691,53	34,79	1507,65	42,83
PP/QF21/N7	PP+QF-300E(21%)[PP-g-MA]+Nano-15(7%)	2021,10	34,10	1655,79	42,53
PP/QF9	PP+ QF-300E(9%)[PP-g-MA]-BLANK	1568,70	33,87	1279,39	39,31
PP/M9/N3	PP+M613-05(9%)[PP-g-MA]+Nano-15(3%)	1889,64	35,55	1534,80	45,05
PP/M15/N5	PP+M613-05(15%)[PP-g-MA]+Nano-15(5%)	2001,58	34,84	1588,36	44,97
PP/M21/N7	PP+M613-05(21%)[PP-g-MA]+Nano-15(7%)	1943,86	34,34	1623,92	44,39
PP/M9	PP+M613-05(9%)[PP-g-MA]-BLANK	1493,25	31,86	1101,07	36,61

Tensile max. stress, i.e., tensile strength and tensile Young's modulus of PP nanocomposites with various organoclay contents were given above. Considering the same processing conditions, the Young's modulus was higher in presence of compatibilizer for all filler contents (3, 5 and 7 wt. %) owing to the greater interaction between filler and polymer matrix. This implies that the stress is much more efficiently transferred from the polymer matrix to the inorganic filler, resulting in a higher increase in tensile modulus.

Accordingly, the tensile modulus of the PP nanocomposites increased monotonously as the organoclay content increases. The nanocomposites with 7 wt% and 5 wt% organoclay loadings which are designated as PP/QF21/N7 and PP/M15/N5 had a tensile modulus of 1,40 times (almost 40%) higher than the neat PP. The significant increase in tensile modulus reasonably comes from the nano-scale dispersion of clay in polymer matrix.

On the other hand, although tensile max. stress, i.e., tensile strength increased with respect to unfilled-neat PP, there was a declining trend as the organoclay content increases for PP nanocomposites containing any of the PP-g-MA compatibilizers.

The flexural data in Table 4.4 indicate a modest improvement, particularly with respect to the tensile modulus. As reported above, as a selected data, the flexural modulus of PP nanocomposites designated as PP/QF21/N7 and PP/M21/N7 increased to 1655,79 and 1623,92 MPa, respectively from 1298,75 MPa of neat PP. These results correspond to 27,5% and 25% increase in flexural modulus for abovementioned PP nanocomposites. That is, with the addition of both the organoclay and the compatibilizer, the flexural modulus has evidently increased. Further, the PP nanocomposites retained their flexural strength or have a slightly improved flexural strength in comparison with the unfilled-neat PP and/or PP blends. Namely, the addition of both the organoclay and the compatibilizer improved the flexural strength significantly.

As a result of mechanical properties, the enhancement of the modulus (tensile/flexural) can be explained as the resistance exerted by MMT layers against plastic

deformation of the polymer. In addition, the stretching resistance of polymer chains with an extended conformation in the gallery also contributed to the modulus enhancement [52-54].

4.1.5. Morphological Characterisation (ESEM)

The dispersion of clay particles in compatibilizer-free PP blend (uncompatibilized sys.) and PP nanocomposite containing QF-300E as a PP-g-MA compatibilizer (designated as PP/QF9/N3) were observed on ESEM micrographs of the samples (see Figures 4.8 and 4.9, respectively). From the microscopic fracture surface observations, it can be seen that without compatibilizer, clay dispersion in PP/N3 is coarse showing large particles. Since, no compatibilizer is added, clay particles dispersion in PP/N3 only results from the compounding process, which led to a micro-composite with micron-sized particles. In general, adding a coupling agent greatly improves clay dispersion by acting as a good dispersant during compounding. Fine clay dispersion is obtained in PP nanocomposite (PP/QF9/N3) with organoclay Nanofil-15 in the presence of the QF-300 E (PP-g-MA) compatibilizer used. High magnification (10000X) SEM micrographs presented in Figure 4.9b revealed that silicate layers were arranged in good order and well-dispersed in the polymer matrix. This observation is also in good agreement with previous XRD result of PP nanocomposite (PP/QF9/N3) which was already stated as *intercalated* structure.

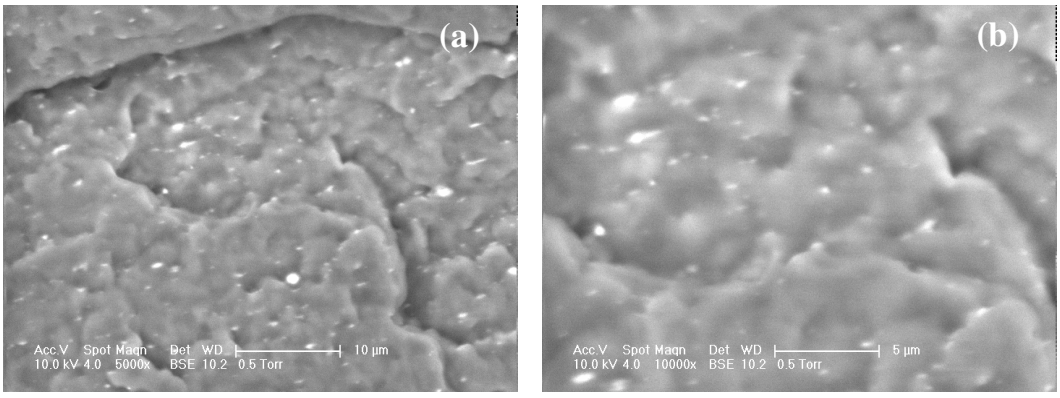

Figure 4.8. ESEM micrograph of cyro-fractured PP/N3 nanocomposite
(a) X5000 magnification and (b) X10000 magnification

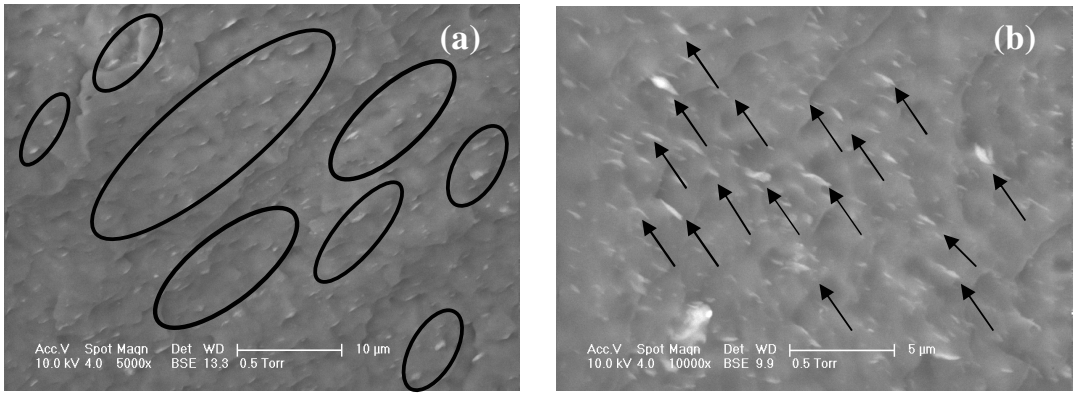

Figure 4.9. ESEM micrograph of cyro-fractured PP/QF9/N3 nanocomposite
(a) X5000 magnification and (b) X10000 magnification

4.1.6. Atomic Force Microscopy (AFM)

In addition to ESEM observations, AFM imaging was carried out to further investigate the dispersion status of the clay in PP matrix. The AFM micrographs of PP nanocomposite in the absence and the presence of compatibilizer QF-300 E were shown in Figure 4.10. Much finer dispersions were found for the corresponding PP nanocomposite containing 3 wt. % of organoclay in the presence of PP-g-MA compatibilizer. This dispersion of much finer particles is the result of *intercalation*, which promotes the regular distribution of silicate particles. In the absence of compatibilizer, it was difficult to

achieve such fine dispersions. It is clear that the presence of PP-g-MA compatibilizer (QF-300 E) improves the dispersion of the ordered nanoclay which was also confirmed by X-ray diffraction analysis.

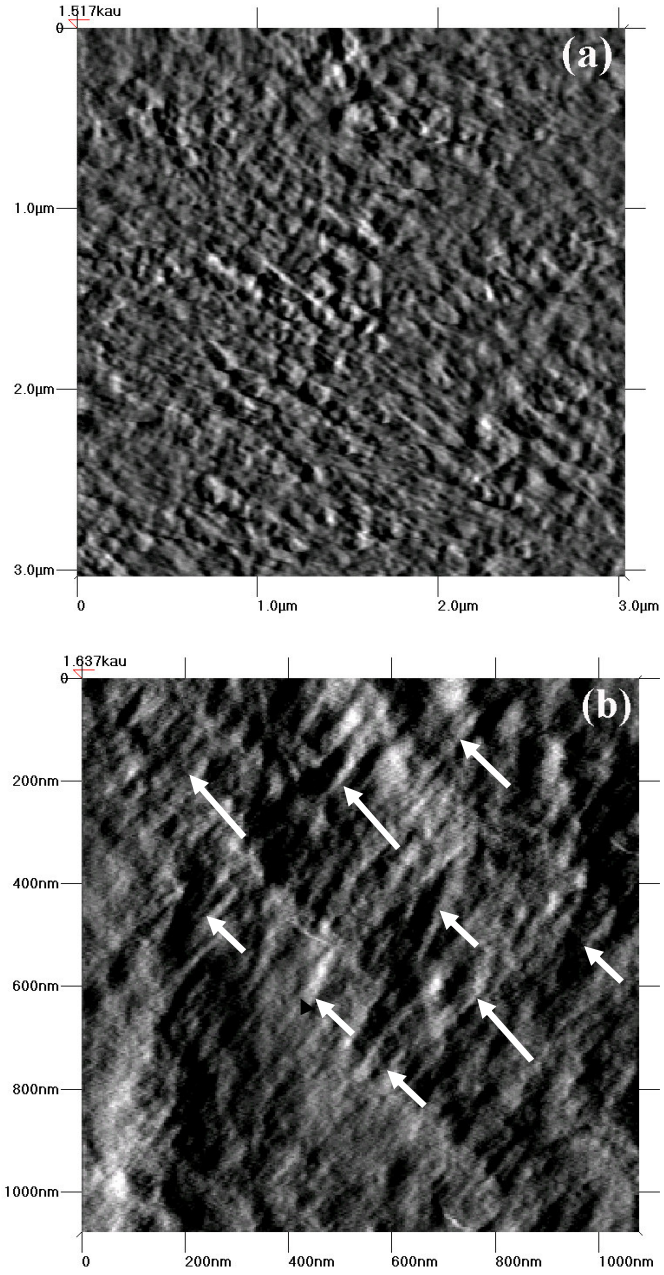

Figure 4.10. AFM images of PP nanocomposite (a) in the absence and (b) in the presence of QF 300E compatibilizer

4.2. Exfoliation Targeted Toughness Enhancement in Polypropylene Layered Silicate Nanocomposites

The synthesis of new exfoliated PP nanocomposites with much more toughened structures via incorporation of maleic anhydride grafted ethylene propylene diene monomer rubber (EPDM-g-MA) as both compatibilizer and toughener is thought to be an original solution to the abovementioned drawbacks.

Some PP/Org-MMT nanocomposites were prepared by using melt blending method. Special attention was paid to the enhancement of clay exfoliation and toughness properties of PP by the introduction of special rubber toughener in the form of compatibilizer in nanocomposite structure. Effects of ratio of toughener-compatibilizer to organoclay as well as organoclay content on dynamic mechanical, thermal and morphological properties of the toughened polypropylene nanocomposites were all discussed in details.

4.2.1. X-Ray Diffraction Analysis (XRD)

XRD is used to examine the intercalation and/or exfoliation of clay through the polymer matrix by monitoring the reflections from the silicate layers. A fully exfoliated nanocomposite would show no peaks in the region 2θ = 1-10 ^{o}, however, an increased *d*-spacing indicates a wider separation of the silicate layers associated with polymer intercalation. XRD patterns of the PP nanocomposites having varying compatibilizer to organoclay ratio (i.e., 1:1, 2:1, 3:1) but fixed organoclay loading (i.e., 3 wt.%) as well as varying organoclay loadings (i.e., 3, 5, 7 wt. %) but fixed compatibilizer to organoclay ratio (i.e., 3:1) are given in Figures 4.11 and 4.12, respectively.

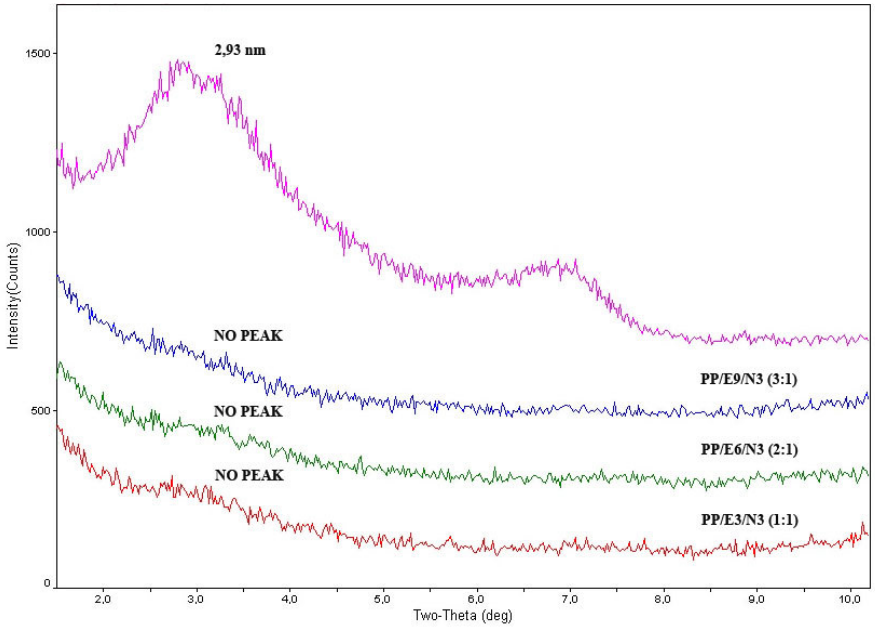

Figure 4.11. XRD patterns of organoclay and 3 wt.% organoclay loaded PP nanocomposites with varying compatibilizer to organoclay ratio (1:1, 2:1, 3:1)

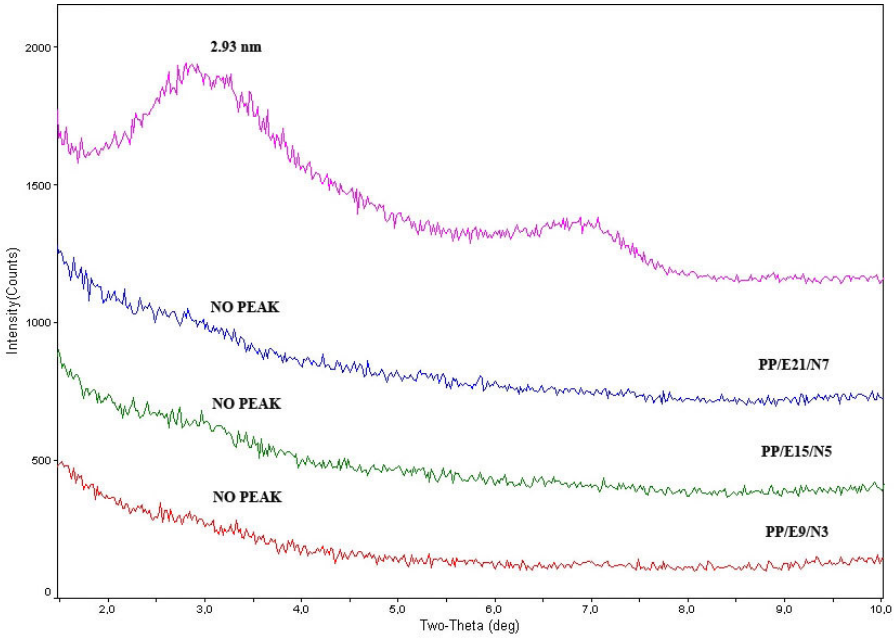

Figure 4.12. XRD patterns of organoclay and PP nanocomposites with constant 3:1 compatibilizer to organoclay ratio and varying organoclay loading (3, 5, 7 wt. %)

As seen in Figures, organophilic MMT has mainly two distinct diffraction peaks corresponding to two populations of MMT with different gallery spacings. However, regardless of the organoclay loading degree and the compatibilizer to organoclay ratio, XRD patterns of all resulting PP nanocomposites containing EPDM-g-MA as a compatibilizer exhibited no diffraction peaks demonstrating the complete delamination or exfoliation of silicate layers in PP matrix [1]. The decrease in intensity and the brodening of peaks also indicate the stacks of layered silicates become more disordered which could be another result of the exfoliation of layered silicates.

4.2.2. Morphological ESEM Analysis

ESEM experiment was carried out to understand the phase morphology of binary blend PP/EPDM-g-MA(9 wt.%) and ternary PP nanocomposite having 3 wt. % organoclay loading and compatibilizer to organoclay ratio of 3:1 given in Figure 4.13a and b, respectively. Dark holes represent the holes resulting from etched EPDM particles in PP matrix. It can be clearly seen that the almost 6-10 μm rubber domain size decreases dramatically to 1-3 μm and even less than 1 μm in the presence of nanolayers. Reduction in the domain size may be attributed to both the nano size directed domain morphology via reduction in the difference in melt viscosities of continuous polymer matrix and dispersed phase [55]. resulting in improvement in the mixing properties gained by the presence of nanosilicate layers, giving a sharper shear-thinning nature to the composites [56] as well as possible agglomeration of the compatible nanolayers around the EPDM particles and forming a diffused layer between PP and EPDM.

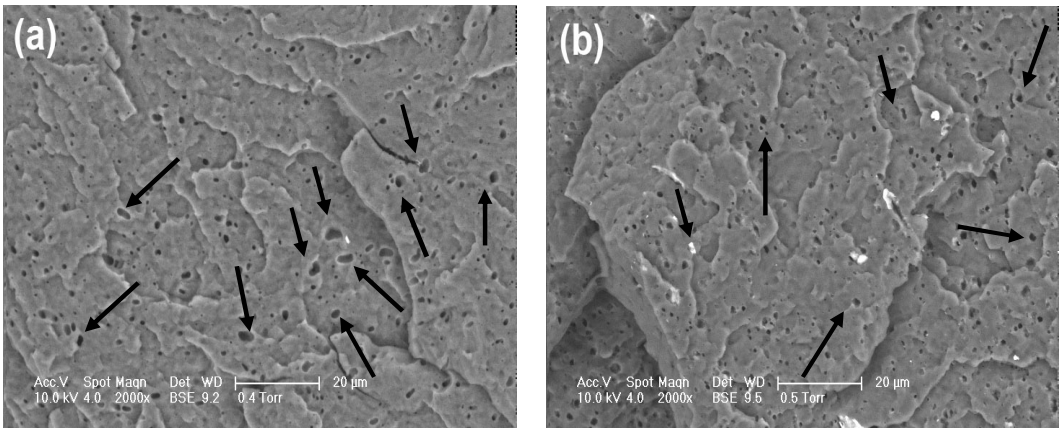

Figure 4.13. ESEM images of etched (a) PP/E9-BLANK and (b) PP/E9/N3 samples.

4.2.3. AFM Analysis

The surface force measurement was applied for the morphological area identification in both binary blend matrices and its nanocomposite form. The adhesion forces were calculated from the force-plots obtained by surface indentation method. During an indentation measurement or a loading/unloading process, the cantilever tip is moved from a certain position down toward the surface by a certain distance Z range (loading) and indentation ends when loading distance (Z) or a specified force has been reached. Then, the tip is moved back up to "unloading position" [57].

Figure 4.14 shows a typical force-loading distance (Z) curve. In a loading/unloading process, the cantilever tip moves back and forth at one fixed point of the sample surface and the forces between tip and surface deflect the cantilever. This gives approaching and retracting curves. In the approaching region, when tip and sample are still far away from each other, the cantilever is at the equilibrium position and the detected force is zero (zero line). On further approach, the cantilever will be deflected by the surface forces. At a certain distance, one can observe an abrupt jump of the tip onto the sample surface that corresponds to a point of discontinuity in the force curve (snap-in). When the distance is further decreased, the tip is pressed against the sample until a defined force value or loading distance is reached. At this point, the direction of the sample motion is inverted and the tip is withdrawn from the sample. At a certain distance the tip detaches from the

sample (snap out) and cantilever comes back to its equilibrium position. A zero force is acquired again (zero line). Force is recorded from sensitivity and deflection of cantilever. The force corresponding to the snap-out is equal to the adhesion force between tip and sample. It is well known that the darkest area, which has a long-range adhesion nature**,** in the images corresponds to the softest phase on the surface [58].

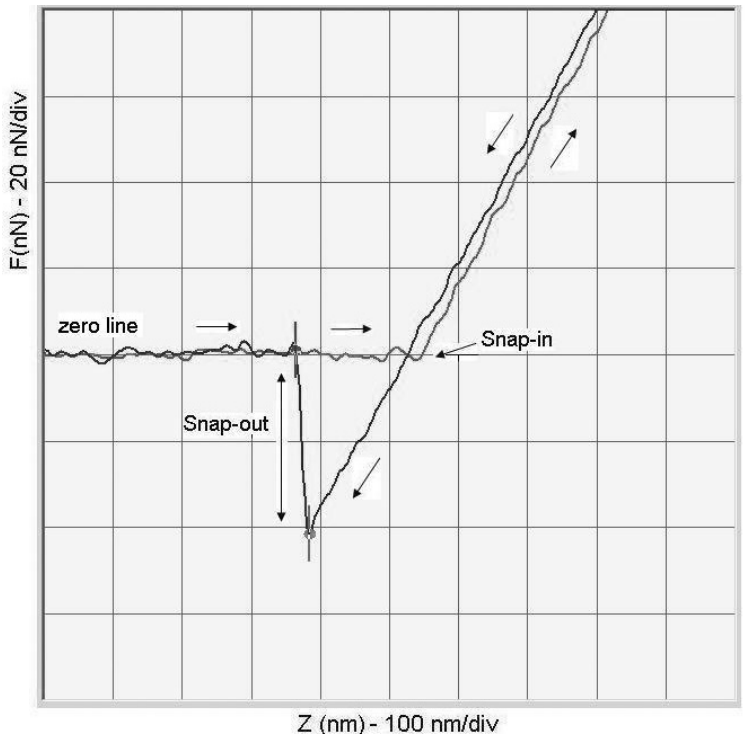

Figure 4.14. A typical force-plot of atomic force microscope.

Figures 4.15 and 4.16 show force-plots from surface indentation measurement which was performed on black, gray and white-colored regions on the Z-height images of selected samples, PP/E9 and PP/E9/N3. Adhesion force values, as determined from the snap-out portion of the retracting curves, were given in Table 4.5. As it can be seen from the Figure 4.15 and Table 4.5 that the maximum snap-out obtained may be resulted from the most adhesive nature of the soft EPDM phase (black-colored) [58]. Relatively, the harder PP phase (gray-colored) was found to have lower adhesion force and the lowest adhesion force value was obtained from the white-colored region of the PP/E9 surface which may be attributed to the maleic anhydride-rich phase.

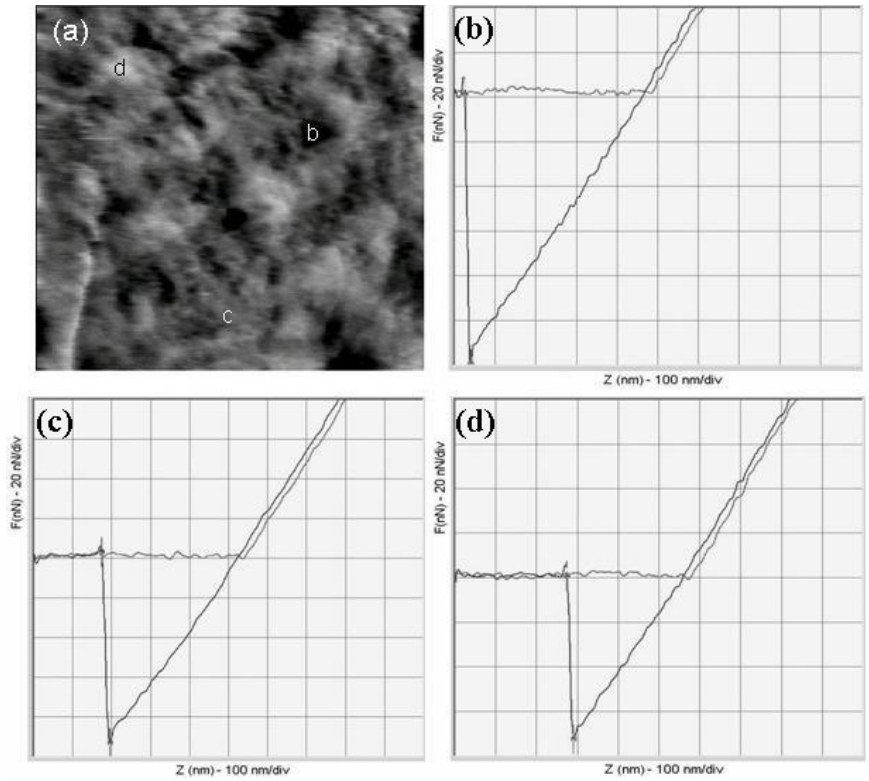

Figure 4.15. Z height-image of PP/E9 sample (scan size-1 µm) and force-plots on soft EPDM block (b), PP phase (c) and maleic anhydride-rich PP phase (d).

Table 4.5. Adhesion forces from force-plots for PP/E9 sample

Sample	Adhesion Force (nN)
EPDM phase in PP/E9	117.9 ± 4.7
PP phase in PP/E9	95.4 ± 9
MA-rich phase in PP/E9	73.1 ± 5.4

On the other hand, the adhesion force values obtained from the surface of PP/E9/N3 nanocomposite (Figure 4.16 and Table 4.6) all reduced to lower values compared to those obtained from PP/E9 surface. The least adhesion force was observed on hard MA-rich PP phase quantifying it to be the most stiff region probably due to high H-bonding type interaction with organoclay in the nanocomposite. This reduction in adhesion force for all phases of PP/E9/N3 sample can be ascribed to homogeneous dispersion of the organoclay in the nanocomposite which is in good agreement with XRD data (Figure 4.11) .

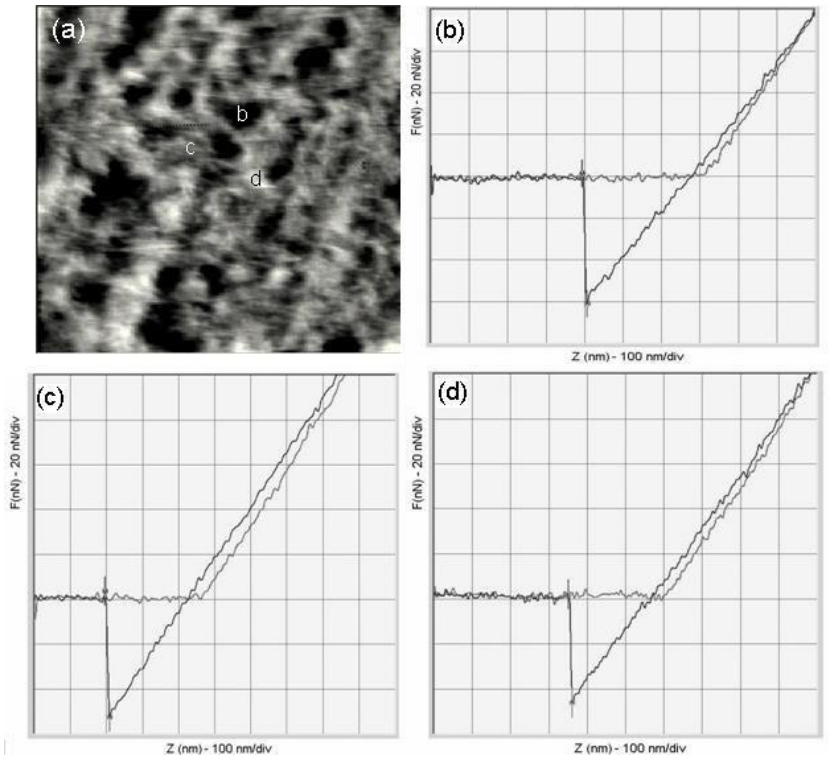

Figure 4.16. Z height-image of PP/E9/N3 sample (scan size-1 µm) and force-plots on soft EPDM block (b), PP phase (c) and maleic anhydride-rich phase (d).

Table 4.6. Adhesion forces from force-plots for PP/E9/N3 sample

Sample	Adhesion Force (nN)
EPDM phase in PP/E9/N3	61.2 ± 1.8
PP phase in PP/E9/N3	56.5 ± 2.1
MA-rich phase in PP/E9/N3	50.6 ± 0.7

In PP/E9 (Figure 4.15), the abovementioned integrated dark rubber domains with a quite large size were found to have a heterogeneous dispersion in PP matrix whereas PP/E9/N3 nanocomposite (Figure 4.16), EPDM domains in the PP matrix were dispersed more homogeneously with a smaller size , probably due to deposition of nanosized silicate platelets selectively around the dispersed rubber phase (Figure 4.17a) and disruption of the continuity of this discrete phase via shear thinning then resulting in smaller domains . Surrounding of rubber domains with nanolayers are believed to be resulted from the strong hydrogen bonding between the hydroxyl groups of silicates and MA groups of rubber. Moreover, the dispersion of the nanolayers in PP matrix is also obvious in magnified image of the nanocomposites (Figure 4.17b)

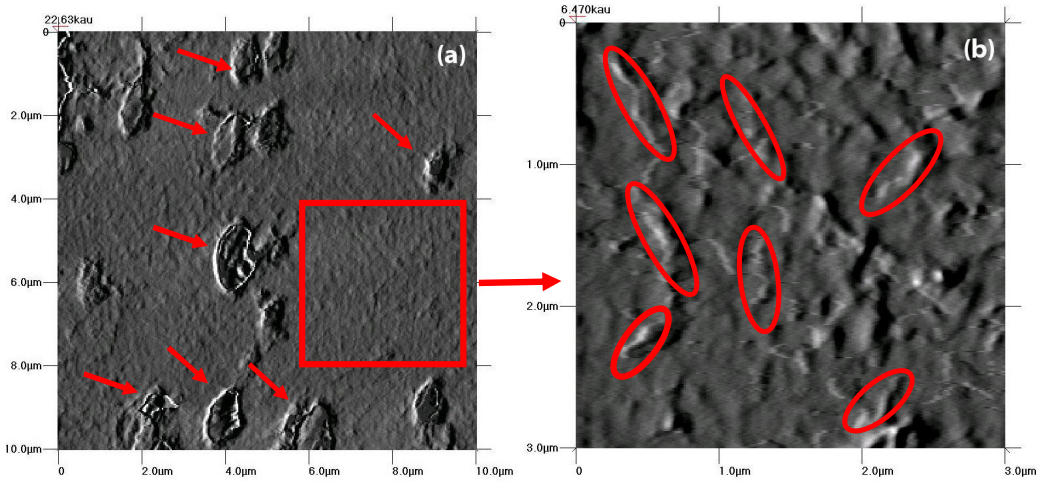

Figure 4.17. AFM phase images of non-etched PP/E9/N3 sample:
Within an area of (a) 10 µm x 10 µm and (b) 3µm x 3µm

In order to emphasize the abovementioned nanosilica morphology, the etched surface of 3 wt.% clay-loaded nanocomposite, PP/E9/N3 was scanned in tapping mode AFM. The nanoscale dispersion in the etched nanocomposite was also easily observed as shown in Figure 4.18.

Exfoliation is quite clear and the silica nanoplatelets with a thickness of *ca* 35 nm are largely separated from each other (*ca* 151.2 nm) and oriented in all possible directions to one another in the matrix as a further confirmation of above mentioned XRD peak disappearance.

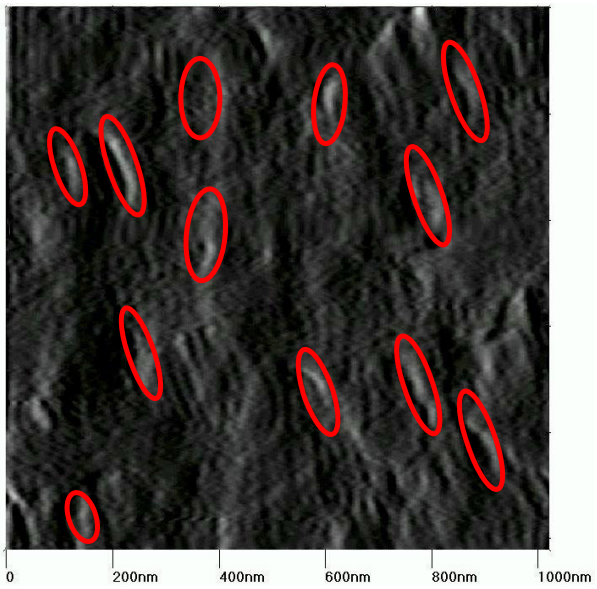

Figure 4.18. AFM phase image of etched PP/E9/N3 nanocomposite

4.2.4. Thermal Stability Test (TGA)

The thermal stabilities of conventional PP, EPDM-g-MA toughened PP binary blank blend and EPDM-g-MA toughened PP nanocomposites with varying compatibilizer to organoclay ratio (i.e., 1:1, 2:1, 3:1) but fixed organoclay loading (i.e., 3 wt.%) as well as varying organoclay loadings (i.e., 3, 5, 7 wt. %) but fixed compatibilizer to organoclay ratio (i.e., 3:1) were all evaluated by TGA and the results were given in Figure 4.19 and 4.20, respectively. It appears that regardless of the organoclay loading degree and the compatibilizer to organoclay ratio all PPNCs exhibited the single decomposition trend and began to decompose at higher temperatures (around 430 ^{o}C) and resulted in higher char contents compared to both neat PP matrix (around 330 ^{o}C) and its binary blend (around 370 ^{o}C). This may be attributed to the compact silica-matrix structure inhibiting heat transfer through composites and slowing down the escaping of volatile degraded products from the system [59].

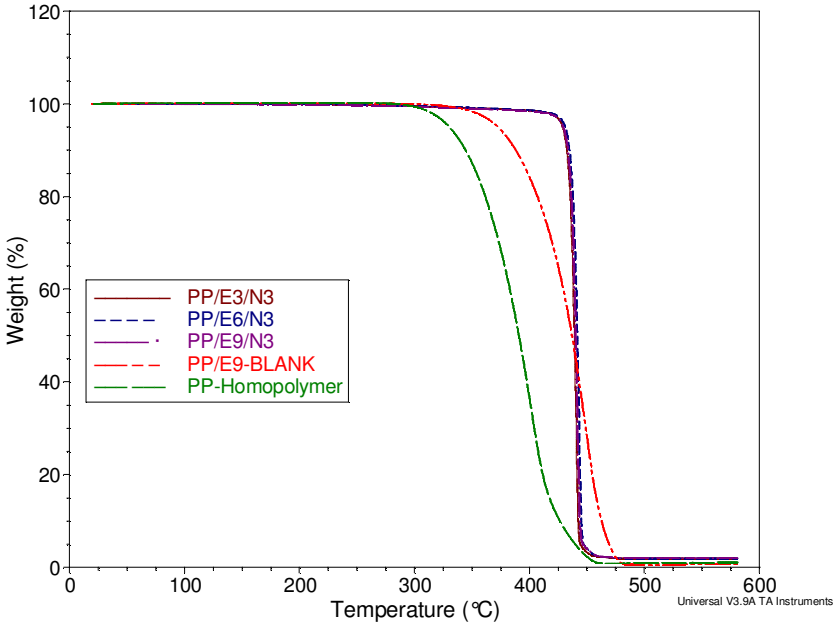

Figure 4.19. TGA curves of neat PP, organoclay-free PP/E(9 %)-Blank Blend and 3 wt.% organoclay loaded PPNCs with varying compatibilizer to organoclay ratio

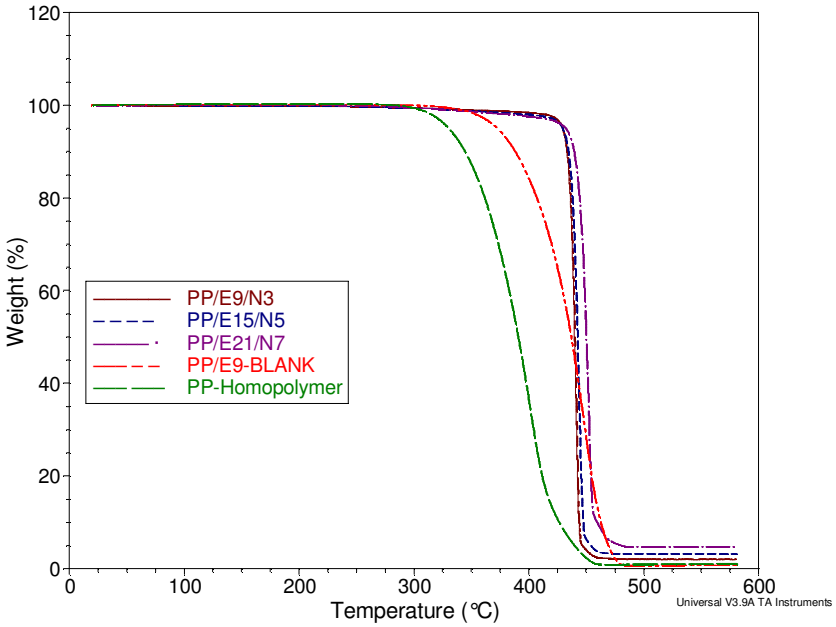

Figure 4.20. TGA curves of neat PP, organoclay-free PP/E(9 %)-Blank Blend and PP nanocomposites with constant compatibilizer to organoclay ratio (3:1) and varying organoclay loadings (3, 5, 7 wt. %)

4.2.5. Dynamic Mechanical Analysis (DMA)

The 3 wt.% organoclay loaded PP nanocomposites with varying compatibilizer to organoclay ratio (1:1, 2:1, 3:1) were also investigated by dynamic mechanical analysis. The tan δ curves of corresponding PP blend and nanocomposites were plotted as a function of temperature shown in Figure 4.21.

Two distinct relaxation temperatures of the elastic rubber phase and rigid PP phase at around -35 °C and 20 °C, respectively, can be seen in Figure 4.21. These peaks are the characteristics of two phase PP-EPDM binary blends. In addition, since PP may crystallize in three different forms such as α, β, γ [29, 60], the maxima at elevated tempareratures (around 80-85 °C) reasonably associated with *β*–relaxations which are related with very small-scale molecular motions.

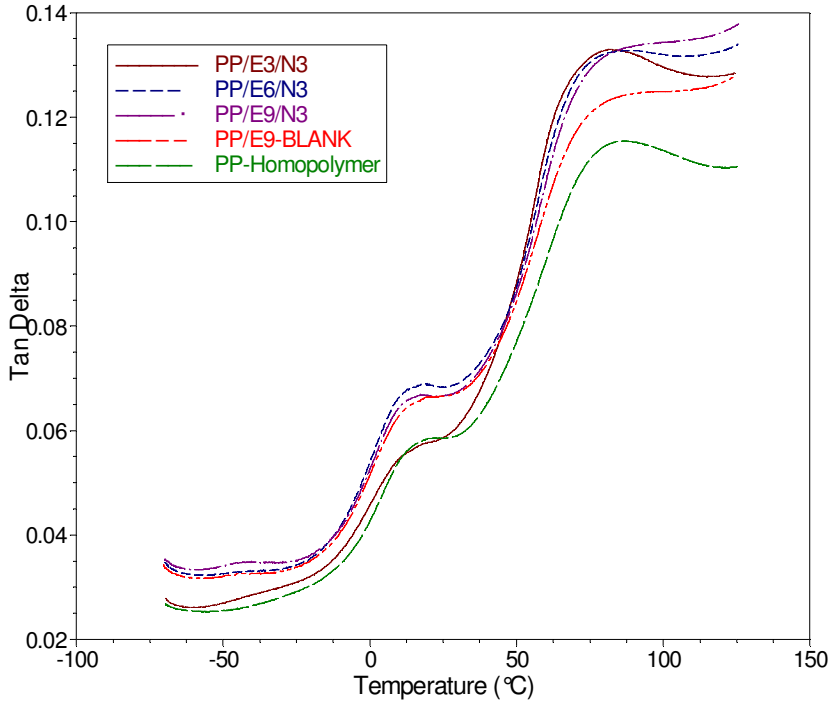

Figure 4.21. Temperature dependency of tan δ at 1 Hz for PP, organoclay-free PP/E(9 %)-Blank Blend and 3 wt.% organoclay loaded PP nanocomposites with varying compatibilizer to organoclay ratio (1:1, 2:1, 3:1)

In nanocomposite formulations, peak values of both EPDM and PP increased to certain extent but this increase is more pronounced in PP. It is well known that the peak value is proportional to the concentration of the component in the composition. The larger increase in the PP peak value indicates that nanolayers are mainly dispersed in PP matrix thus increasing the effective volume of PP which can be further confirmed by larger increase of T_g of PP owing to the influence of nanolayers on the mobility of PP and EPDM chains [61]. Additionally, increase in EPDM peak intensity as well as constant EPDM peak position (T_g) can only be explained by the seldom dispersion of nanolayers in EPDM phase but rather most of them are concentrated around the EPDM phase resulting in increase of the effective volume of EPDM and at the same time nanolayers spread over PP matrix effectively decreasing the mobility of PP chains.

Moreover, the loss factor (tan δ) is one of the damping parameters since it is measure of ability of the polymer to convert mechanical energy into heat as damping at a temperature or frequency of interest. As it can be seen from the figure nanocomposites showed quite broad damping temperature range in which the material can act as effective damper.

4.2.6. Izod Impact Strength Measurements

The change of impact strength as a function of loading degree as well as compatibilizer to organoclay ratio in PP nanocomposites compared to neat PP and organoclay-free PP/E9-Blank Blend have been evaluated and the data is given in Table 4.7.

In general, the presence of compatibilizer and organo-nanoclay increases the impact strength, possibly due to modification of the matrix morphology [62]. In addition, the clay may absorb the impact energy and slow down the crack propagation. During impact, the stress in the sample may be dispersed by exfoliated layers, which have higher strength and modulus than the matrix, thus making the Izod impact strength higher.

Table 4.7. Izod Impact Strength of the neat PP, organoclay-free PP/E9-Blank Blend and PP nanocomposites

SAMPLES	NOTCHED IZOD IMPACT STRENGTH (kJ/m^2)
PP	2,89
PP/E9	3,70
PP/E3/N3	3,49
PP/E6/N3	3,93
PP/E9/N3	4,17
PP/E5/N5	3,41
PP/E10/N5	3,83
PP/E15/N5	4,91
PP/E21/N7	6,13

It is interesting that the impact strength of PP is remarkably enhanced by almost 112 % by both elastomeric compatibilizer and organo-nanoclay addition. It is known that the bimodally distributed rubber particle size has a key role in the enhancement of toughness especially if the most rubber particles have less than 1 μm in size [63]. Okamato [64] suggested that the long extended crazes were induced by the large particles overlapped by the crazes from small particles in the vicinity of the large particles, leading to higher impact strength. In the nanocomposites prepared in this study, dramatic increase observed in toughness values are most probably resulting from the decreased rubber domain size of *ca* less than 1 μm acting as abovementioned synergism creating small and large domains. Moreover, this synergetic effect may also be attributed to the decrease in interparticle distance and overlap of the stress field between EPDM and silica nanolayers leading to the percolation of the stress field in the entire PP matrix [61]. Additionally, the enhancement of Izod impact strength is also more probably due to the fact that the exfoliated clay layers in nanocomposite play a role in hindering the crack path caused by impact.

5. CONCLUSIONS

Polypropylene nanocomposites (PPNCs) using the commercial organoclay and PP-g-MA and EPDM-g-MA compatibilizers were prepared successfully by melt blending in a twin-screw extruder. The effect of layered silicate and compatibilizers on the nanocomposite structure in terms of clay dispersion, intercalation/delamination, and morphology as well as physical, thermal, and static/dynamic mechanical properties was studied extensively.

In the first part of the study, the degree of dispersion was improved by incorporating maleic anhydride grafted polypropylene (PP-g-MA) as a compatibilizer. The use of PP-g-MA compatibilizer led to generally *intercalated* nanocomposites as confirmed by XRD results with increased *d*-spacing shifting towards lower 2θ angles. Depending on the characteristics of the PP-g-MA coupling agent such as molecular weight and MA grafting content, different extent of clay intercalation was reached.

The use of PP-g-MA with low molecular weight and high MA grafting content (i.e., FUSABOND-M 613-05) led to relatively good and uniform intercalation especially in the PP nanocomposite designated as PP/M15/N5 (d_{001} = 2,97 nm). Such PP-g-MA could interact largely with clay particles and intercalate easily into the clay platelets. However, the lack of miscibility with PP matrix could explain why further larger intercalation can not be achieved.

The use of PP-g-MA with high molecular weight and low MA grafting content (i.e., ADMER-QF-300 E) led to more heterogeneous intercalation with more distanced layers structure especially in the PP nanocomposite designated as PP/QF15/N5 (d_{001} = 3,15 nm). Such PP-g-MA could interact to a lesser extent with clay due to its lower grafting content leading to some limited intercalation. However, its higher molecular weight (Mwt) and better miscibility with PP probably allowed some larger level of intercalation to be achieved.

Moreover, regardless of the type of PP-g-MA used, all PP nanocomposites exhibited enhanced thermal stability, and better static (namely; tensile and flexural) and dynamic properties (i.e., the storage modulus) compared to neat PP matrix.

As a result, finely dispersed intercalated silicate layers throughout the PP matrix were evidently responsible for those improved properties.

In the second part of the study, both exfoliated and toughened polypropylene nanocomposites were prepared by melt extrusion in a twin screw extruder. Special attention was paid to the enhancement of clay exfoliation and toughness properties of PP by the introduction of a rubber in the form of compatibilizer toughener–maleic anhydride grafted ethylene propylene diene monomer rubber (EPDM-g-MA). It has been found that the desired exfoliated nanocomposite structure could be achieved in all compatibilizer to organoclay ratios (i.e., 1:1, 2:1, 3:1) as well as clay loadings (e.g, 3, 5, 7 wt.%). Moreover mechanism with decreased size of rubber domains surrounded with nanolayers as well as exfoliation of the nanolayers in PP matrix was found to be responsible from dramatic increase in impact resistance of nanocomposites. That is, elastomer particles might play the role of craze-inducing agent, and caused shear yielding of the surrounding matrix and terminated the propagation of cracks. Additionally, improved thermal and dynamic mechanical properties of the resultant nanocomposites promised to open a new way for highly toughened super PPs via nanocomposite assemblies even with a very low loading degrees.

REFERENCES

1. Alexandre, M. and P. Dubois , "Polymer-layered Silicate Nanocomposites: Preparation, Properties and Uses of a New Class of Materials", *Material Science and Engineering*, Vol. 28, pp. 1-63, 2000.

2. Theng, B.K.G., *The Chemistry of Clay-Organic Reactions*, Wiley, New York, 1974.

3. Ogawa, M. and K. Kuroda , "Preparation of inorganic-organic nanocomposites through intercalation of organoammonium ions into layered silicates", *Bull. Chem. Soc. Japan*. Vol. 70, 2593-2618, 1997.

4. Blumstein, A., "Polymerization of adsorbed monolayers: II.Thermal degradation of the inserted polymers." *J Polym Sci A* ,Vol. 3, pp. 2665-2673, 1965.

5. Carter, L., J. G. Hendricks and D. S. Bolley, US 2,531,396; 1950 [assigned to National Lead Co.].

6. Ray, S. S. and M. Okamoto, "Polymer/Layered Silicate Nanocomposites: A Review From Preparation to Processing", *Progress in Polymer Science*, Vol. 28, pp. 1539-1641, 2003.

7. LeBaron, P. C., Z. Wang and T. J. Pinnavaia, *Appl Clay Sci*,Vol.15: 11–29, 1999.

8. Pinnavaia, T. J. and G. W. Beall, *Polymer-clay nanocomposites*. Baffin Lane: Wiley; 2001.

9. Usuki, A., Y. Kojima, M. Kawasumi, A. Okada, Y. Fukushima, T. Kurauchi and O. Kamigaito, *J Mater Res* ,Vol. 8, 1179, 1993.

10. Kojima, Y., A. Usuki, M. Kawasumi, A. Okada, T. Kurauchi and O. Kamigaito, *J Polym Sci Part A: Polym Chem,* Vol. 31, 983, 1993.

11. Lagaly, G., in: *"Development in Ionic Polymers"*, A. D. Wilson, H. T. Posser, Eds., Applied Science Publishers, London, chapter 2, p. 77, 1986.

12. Akelah, in: *"Polymers and Other Advanced Materials"*, N. Prasad, J. E. Mark, T. J. Fai, Eds., Plenum Press, New York, p. 625, 1995.

13. Giannelis, E.P., *Adv. Mater.* Vol.**8**, p.29, 1996.

14. Pinnavaia, T. J., T. Lan, Z. Wang, H. Shi and P. D. Kaviratna, in: *"Nanotechnology",* G. M. Chow, K. E. Gonsalves, Eds., American Chemical Society, Washington, *ACS Symp. Ser.* 622, 251, 1996.

15. Zilg, C., Reichert P., Dietsche F., Engelhardt T. and Mülhaupt R., *Kunststoffe,* Vol. 88, 1812, 1998.

16. Charles, E., *The Chemistry of Clay Minerals*; Elsevier: Amsterdam; p 20. 1973.

17. Theng, B.K.G., *Formation and properties of clay–polymer complexes*. Amsterdam: Elsevier; 1979.

18. Vaia, R. A., H. Ishii and E. P. Giannelis, "Synthesis and properties of two-dimensional nanostructures by direct intercalation of polymer melts in layered silicates", *Chem Mater* ,Vol. 5: 1694–6, 1993.

19. Brindly, S. W. and G. Brown (editors), *Crystal structure of clay minerals and their X-ray diffraction.* London: Mineralogical Society; 1980.

20. Aranda, P. and E. Ruiz-Hitzky, "Poly(ethylene oxide)-silicate intercalation materials", *Chem Mater*, Vol. 4:1395–403, 1992.

21. Greenland, D. J., "Adsorption of poly(vinyl alcohols) by montmorillonite", *J Colloid Sci.* Vol. 18: 647–64, 1963.

22. Krishnamoorti, R., R. A. Vaia and E. P. Giannelis, "Structure and dynamics of polymer-layered silicate nanocomposites", *Chem Mater* , Vol. 8: 1728–34, 1996.

23. Kornmann, X., "Synthesis and Caracterisation of Thermoset-Clay Nanocomposites", Division of Polymer Engineering, Lulea University of Technology, Sweden

24. Lagaly, G., "Interaction of alkylamines with different types of layered compounds", *Solid State Ionics*, Vol. 22: 43–51, 1986.

25. Yano, K., A. Usuki, A. Okada, T. Kurauchi and O. Kamigaito, "Synthesis and properties of polyimide–clay hybrid", *J Polym Sci, Part A: Polym Chem,* Vol.31: 2493–8, 1993.

26. Kojima, Y., A. Usuki, M. Kawasumi, A. Okada, Y. Fukushima, T. Kurauchi and O. Kamigaito, "Mechanical properties of nylon 6–clay hybrid", *J Mater Res*, Vol.: 1185–9, 1993.

27. Fukushima, Y., A. Okada, M. Kawasumi, T. Kurauchi and O. Kamigaito, "Swelling Behaviour of Montmorillonite by Poly-6-Amide", *Clay Miner*, Vol. 23, No. 1, pp. 27-34, 1988.

28. Usuki, A., Y. Kojima, M. Kawasumi, A. Okada, Y. Fukushima and T. Kurauchi, "Synthesis of Nylon 6-Clay Hybrid", J. *Mater. Res.*, Vol. 8, No. 5, pp. 1179-1184, 1993

29. Moore, E. P., *Polypropylene Handbook*; Hanser: Munich, 1996.

30. Usuki, A., M. Kato, A. Okada and T. Kurauchi, "Synthesis of Polypropylene-Clay Hybrid", *J. Appl. Polym. Sci.*, Vol. 63, pp. 137-139, 1997.

31. Kawasumi, M., N. Hasegawa, M. Kato, A. Usuki and A. Okada, "Preparation and Mechanical Properties of Polypropylene-Clay Hybrids", *Macromolecules*, Vol. 30, pp. 6333-6338, 1997.

32. Nam, P. H., P. Maiti, M. Okamoto, T. Kotaka, N. Hasegawa and A. Usuki, *Polymer,* Vol.42: 9633-40, 2001.

33. Kato, M., A. Usuki and A. Okada, *J Appl Polym Sci.*,Vol. 66: 1781-5, 1997.

34. Reichert, P., H. Nitz, S. Klinke, R. Brandsch, R. Thomann and R. Mülhaupt, *Macromol Mater Eng*, Vol. 275, 8, 2000.

35. Ishida, H., S. Campbell and J. Blackwell, *Chem Mater*, Vol. 12: 1260, 2000.

36. Utracki, L. A., In *Polypropylene: A–Z Reference*; Karger-Koccis, K., Ed.; Kluwer: Dordrecht, p 621, 1999.

37. Lim, J. W., A. Hassan, A. R. Rahmat and M. U Wahit, *Polym.Int.,* Vol. 55: 204, 2006.

38. Tjong, S. C., Xu, S. A., Li, R. K. Y., Mai, Y. W., *J Appl Polym Sci.*, Vol. 86: 1303, 2002.

39. Tjong, S. C. and Bao S. P., "Fracture Toughness of High Density Polyethylene/SEBS-g-MA/Montmorillonite Nanocomposites", *Composites Science and Technology*, Vol. 67, pp. 314-323, 2007.

40. Tjong, S. C., and Y. Z. Meng, "Impact-Modified Polypropylene/Vermiculite Nanocomposites", *J. Polym. Sci.: Part B: Polymer Physics*, Vol. 41, pp. 2332-2341, 2003.

41. Li, Y. M., G. Xue and H. J. Sue, "Morphology and toughening mechanisms in clay-modified styrene–butadiene–styrene rubber-toughened polypropylene." *J Mater Sci.*, Vol.37: 2447–59, 2002.

42. Zhu, L., and M. Xanthos, "Effects of Process Conditions and Mixing Protocols on Structure of Extruded Polypropylene Nanocomposites", *J. Appl. Polym. Sci.*, Vol. 93, pp. 1891-1899, 2004.

43. Zeus Technical Whitepaper, "Melt Extrusion: The Basic Process", Zeus Industrial Products, Inc., 2006.

44. Rauwendaal, C., *Polymer Extrusion*, Hanser Gardner Publications, Munich, 2001.

45. Raman, V. C., Y. Jaluria, M. V. Karwe and V. Sernas, *Polym. Eng. Sci.*, Vol. 36, No. 11, pp. 1531-1540, 1996.

46. Prat, L., S. N'Diaye, L. Rigal, C. Gourdon, "Solid-Liquid Transport in a Modified Co-rotating Twin-Screw Extruder_Dynamic Simulator and Experimental Validations", *Chem. Eng. Process.,* Vol. 43, pp. 881-886, 2004.

47. ISO R527-1966 (E), "Plastics – Determination of Tensile Properties", International Organization for Standardization, 1966.

48. ISO 178-1975 (E), "Plastics – Determination of Flexural Properties of Rigid Plastics", International Organization for Standardization, 1975.

49. ISO 180-1982 (E), "Plastics – Determination of Izod Impact Strength of Rigid Materials", International Organization for Standardization, 1982.

50. Kim, K. N., H. S. Kim and J. W. Lee, *Polym Eng Sci*., Vol. 41: 1963, 2001.

51. Perrin-Sarazin, F., M.-T. Ton-That, M. N. Bureau, and J. Denault, "Micro-and nano-structure in polypropylene/clay nanocomposites", *Polymer,* Vol. 46: 11624-11634, 2005.

52. Lee, D. C. and L. W. Jang, *J Appl Polym Sci*., Vol. 61: 1117, 1996.

53. Lee, D. C. and L. W. Jang, *J Appl Polym Sci*., Vol. 68: 1997, 1998.

54. Jang, L. W., C. M. Kang and D. C. Lee, *J Polym Sci Part B: Polym Phys*., Vol. 39: 719, 2001.

55. Wang, Y., F. B. Chen, Y. C. Li and K. C. Wu, *Compos. B.* Vol. 35: 111, 2004.

56. Dazhu, C., Y. Haiyang, H. Pingsheng and Z. Weian, *Composites Science and Technology*, Vol. 65: 1593, 2005.

57. USPM Instruction Manual Version 5, Santa Cruz, CA, USA, Ambios Technology, 2007

58. Ganguly, A., M. De Sarkar and A. K. Bhowmick, *Journal of Polymer Science: Part B: Polymer Physics*, Vol. 45: 52, 2007.

59. Sen, S., N. Nugay and T. Nugay, *Polymer Int*., Vol**.** 55: 552, 2006.

60. Marega, C., A. Marigo, G. Cingano, R. Zannetti and G. Paganetto, *Polymer*, Vol. 37: 5549, 1996.

61. Yang, X., Zhang, C., Qu, Bo., Li, L., Zhang, Q. and Q. Fu. Zhang, *Polymer*, Vol. 48: 860, 2007.

62. Perrin-Sarazin, F., M.-T. Ton-That, M. N. Bureau and J. Denault, "Polyolefin Nanocomposites: Micro-nanostructure Analysis," *Proc. Second International Symposium on Polymer Nanocomposites Science and Technology*, Paper No. 79, Boucherville, Quebec, Canada (Oct. 6-8, 2003).

63. Park, J. Y. and P. O. Ok, *Adv Polym Technol*, Vol. 15(2): 145–50, 1996.

64. Okamoto, Y., H. Miyagi, M. Kakugo and K. Takagashi, *Macromolecules,* Vol. 24: 5639, 1991.